Late Quaternary aeolian environments, luminescence chronology and climate change for the Monahans dune field, Winkler County, West Texas, USA

Keywords: aeolian stratigraphy, OSL dating, Quaternary climate change, TT-OSL, Monahans **Abstract** (250 words)

Dune fields on the Southern High Plains such as the Monahans in West Texas are archives of Quaternary environmental variability. Stratigraphic analyses and sixty-one optically stimulated luminescence (OSL) ages from seven Geoprobe cores and one section from the Monahans reveal a ~550 ka old aeolian sedimentary record with seven carbonate/argillic paleosols and a playa-lake margin deposit. OSL ages on quartz-grains from aeolian sediments by two protocols, single aliquot regeneration (SAR) and thermal transfer (TT), yield congruent ages between 50 and 250 ka, and the oldest ages of ca. 550 ka, potentially minima. This chronostratigraphic analysis and finite-mixture modeling of the OSL-age distribution identify four aeolian depositional periods (ADP) at 545 to 475, 300 to 260, 70 to 45, and post 16 ka and possibly two additional ADPs 460 to 420 ka and 350 to 320 ka. Playa lake deposits identified west of the Monahans and correlative to carbonate-rich paleosols indicate that wetter conditions prevailed during interglacial MIS 7, 235 to 195 ka. Another wetter period, 25 to 16 ka, with the formation of Lake King in the adjacent Rio Grande Valley is correlative with a pedogenicallymodified < 2 m-thick aeolian sand. This study underscores that there may be multiple climatic states, during glacials and interglacials, associated with wetter conditions. In turn, the thickest, preserved aeolian deposits are associated with transitional climate periods, penecontemporaneous with stadials, when the Laurentide ice sheet was < 80% of the last glacial maximum volume, with precipitation-bearing zonal circulation shifted northward and weakened meridional moisture flux.

1.0 Introduction

Quaternary dune fields abound on the Southern High Plains (SHP) USA, with the most southern and driest areas showing contemporary aeolian activity (Carlisle and Marrs, 1982; Muhs and Holliday, 1995) (Fig. 1). These extensive aeolian deposits are associated with fluvial systems, such as the Pecos River, and reflect complex association between sediment supply and availability, climatic forcing, and edaphic associations in the Late Pleistocene and Holocene (e.g., Forman et al., 2001; Muhs et al., 2003; Halfen and Johnson, 2013; McKean et al., 2015). A common Pleistocene deposit on the SHP is the Blackwater Draw Formation (BWD) which infills valleys and is broadly distributed as aeolian sediments in west Texas and adjacent New Mexico (Fig. 1). This Formation is composed of fluvial, aeolian, and playa-like sediments and interbedded with as many as six carbonate-rich paleosols (Holliday, 1989; 1995; Rich and Stokes, 2011; Baird, 2015; Stine et al., 2020). The BWD is widespread at the surface and was a source for Holocene aeolian sands (Holliday, 1989; Muhs and Holliday, 2001; Rich, 2013). The Holocene sands, BWD sediments, and intercalated buried soils reflect changes in available moisture during Pleistocene glacial and interglacial conditions in this semi-arid environment (e.g., Holliday, 1989; 1995; Muhs and Holliday, 2001; Rich and Stokes, 2011; Schmidt and Hertzberg, 2011; Stine et al. 2020).

The base of the BWD may date to the earliest Pleistocene based on fission-track and 40 Ar/ 39 Ar ages on ash and paleomagnetic polarity inferences (Holliday, 1989; 1995; Holliday et al., 2008; Rich and Stokes, 2011; Stine et al., 2020). The Guaje Ash, within the lower section of the BWD, yielded 40 Ar/ 39 Ar ages of 1.61 Ma with an inferred age for the Formation base of ca. 2.0 Ma (Izett et al., 1972; Holliday, 1989; 1991; 1995; Izett and Obradovich, 1994; Gustavson, 1996; Stine et al., 2020). The identification of the Brunhes-

Matuyama geomagnetic polarity reversal event (0.781 Ma) and the Lava Creek B ash (0.631 Ma) within the BWD provides further chronologic control for Late Pleistocene aeolian deposition (Izett et al., 1972; Holliday, 1989; Izett and Obradovich, 1994; Matthews et al., 2015; Suganuma et al., 2015; Stine et al., 2020).

The advent of luminescence dating of quartz grains has provided greater chronologic definition for the upper BWD and overlying Holocene sands. A landmark study by Rich and Stokes (2011) used optical dating of quartz in various dune fields in West Texas, including Muleshoe, Lea-Yoakum, Mescalero, and Monahans dunes (Fig. 1) to show episodic, Late Pleistocene to Holocene depositional history of the upper BWD, with the oldest age of 204 ± 22 ka on quartz grains from the Monahans dune field. Recently, infrared stimulated luminescence dating of feldspar grains from upper part of the BWD, near the type section in Lubbock County, TX, yielded older depositional ages of 294 ± 32 ka and 347 ± 40 (Hall and Goble, 2020). Related studies of the Mescalero sand sheet in adjacent New Mexico have revealed a period of aeolian deposition spanning ~90 to 70 ka, burying a well-developed Mescalero soil, with stage 3 to 4 soil carbonate morphologies (Hall and Goble, 2006; 2015; Hall et al., 2010). There is widespread evidence from OSL ages on quartz grains and radiocarbon dating of included organic matter for numerous phases of Holocene aeolian activity in eastern Mexico and adjoining areas. The latest aeolian deposits are < 200 years old, associated with anthropogenic activity (Hall and Goble, 2006, 2015; Hall et al., 2010; Rich and Stokes, 2011).

The chronologic resolution for the BWD between ca. 700 and 50 ka is limited by the dearth of ages in a well-documented stratigraphic context. Thus, it is difficult to assess the associated changes in geochemistry, pedogenesis, and aeolian deposition with Late Pleistocene climate variability (Wilkens and Currey, 1997; Stokes and Rich, 2011; Rich, 2013; Stine et al., 2020).

This study evaluates the suitability of two optically stimulated luminescence methods, thermal-transfer (TT-OSL) and single aliquot regeneration (OSL-SAR) of quartz grains from sediment cores of the BWD in and adjacent to the Monahans dune field in West Texas (Fig. 1; Table 1). The consistency of TT-OSL dating of quartz grains is evaluated against corresponding OSL-SAR ages between \sim 250 and 50 ka and is permissive due to the relatively low environmental dose rate (D_r , < 1 mGy/y). The developed TT-OSL protocols were also used to date the oldest and deepest sediments, yielding apparent ages between 550 and 500 ka. This enhanced chronology with sedimentologic interpretations provides insights into the factors that drive Late Pleistocene aeolian deposition in the Monahans dune field and broadly on the Southern High Plains.

1.2 Geomorphic, Stratigraphic and Sedimentologic Framework

The Monahans dune field is a perched and isolated aeolian system about 60 km northeast of the Pecos River (Fig. 1). A low relief aeolian sand sheet with parabolic dunes surrounds the Monahans dune field and may be regionally extensive (Hall and Gobles, 2012; 2015) from which Geoprobe cores were extracted for this study (Fig. 1). Cores were taken from these surfaces because of ease of access and a lower water table allowed retrieval of sediment from depths of > 10 m. Seminal stratigraphic studies of the Monahans recognized two informal formations, Judson and Monahans, of aeolian origin (Huffington and Albritton, 1941), which in practice are difficult to differentiate with intercalated carbonate paleosols and playa lake deposits (Green, 1961). The BWD with the type locality near Lubbock, TX, is commonly a valley fill deposit and may extend southward to the Monahans dune field where the aeolian dune and sand sheet facies dominate (Muhs and Holliday, 2001) (Fig. 1). Many

dune fields and sand sheet deposits in far west Texas and adjacent New Mexico and Mexico may be time-equivalent with the BWD (Fig. 1). In this area there are numerous prominent, composite carbonate/argillic soils and buried soils in the near surface intercalated with aeolian sand sheet deposits that yield OSL ages between ca. 100 and 12 ka; and capped by Holocene aeolian sands and coppice dunes, reworked from subjacent older sediment, possibly time-equivalent to the BWD (Holliday, 1989; 1995; Gustavson, 1996; Hall and Gobles, 2012; 2015)

The aeolian stratigraphic record from any one sediment core, particularly for an active dune field like the Monahans is highly incomplete and may reflect a selected record of preserved sediments and paleosols (e.g., Stokes and Bray, 2005; Stauch, 2019). Most of the geologic time in aeolian depositional sequences is represented by erosional unconformities and the intervening periods of pedogenesis on timescales of 10² to 10⁵ yr, reflecting wetter, vegetated, and more stable surface conditions (Cosgrove et al., 2022). Soil development preserved in this stratigraphic context often reflects catenary variations, cumulic-type soil morphologies with aeolian additions, "welding" of numerous periods of pedogenesis, separated by relatively thin (< 1 m) aeolian sediments and differential amounts of erosional truncation (e.g., Ruhe and Olson, 1980; Olson and Nettleton, 1998; Kemp, 2001). The formation of > 0.5 m thick carbonate (stage 2-4) and/or argillic horizon in the Monahans setting yield erosion-resistant levels, which enhance in places the preservation of certain pedosedimentary facies. An important and common process in active dune systems is lateral erosion, truncation and reworking of previously deposited sand that significantly reduces the preservation of the prior depositional record. Reworked aeolian sands are well recognized in the BWD and Holocene aeolian sands (Holliday, 1989; 1995; Gustavson, 1996). Episodes of heightened aeolian activity, dominated by erosion, may be obscured in the stratigraphic record, particularly if the system is sediment starved. Thus, there

are numerous environmental factors such as variable wind speed, sediment supply and availability, groundwater level, and stratigraphic armoring by paleosols that control the preservation of aeolian sediments and the nature of the stratigraphic record (Stauch, 2019).

Previous studies of the BWD indicated that these strata may preserve at least fourteen buried soils, mostly with calcic and argillic morphologies (e.g., Holiday, 1989; Gustavson and Holliday, 1999; Forman et al., 2019; Mayhack, 2021). This analysis of the seven Geoprobe cores, 7 to 19 m long, has identified four aeolian pedosedimentary facies, which excludes the Quarry section because of its unique shallow lacustrine features (Figs. 2 and 3) (Forman et al., 2019; Mayhack, 2021). Facies A is interpreted as aeolian-reworked sediments from the BWD and often occurs in the upper 2 to 4 m in cores. This facies (A) is orange to yellowish brown, well-sorted, medium to fine sand reflecting sand sheet to interdunal sedimentation (Fig. 2). In contrast, Facies B was pale yellowish-brown to gray in color, very well sorted medium sand interpreted as primary aeolian sand, associated with dune accretion. This facies (B) is > 5 m thick and appears massive with zones of centimeter to millimeter bedding. Facies C is characterized by a mostly massive, well sorted, medium to fine aeolian sand dominated by calcareous filaments and nodules associated with stage 1 to 4 soil carbonate morphologies (Birkeland, 1999; p. 356-359). Often the upper 2 m of Facies C sediment is dominated by a truncated, well-developed buried soil with stage 2 to 4 carbonate morphologies, with induration in places (Fig. 2). The pedosedimentary environment of Facies C is associated with limited aeolian sand deposition (< 2 m thick) and more available surface moisture, resulting in relatively stable landforms with carbonate soil formation over variable and long periods of time (10³ to 10⁵ years). Facies D is a moderately well-sorted, light brown to yellow, silty sand to sandy silt. This facies (D) sediments exhibit a variable accumulation

of aeolian sands < 1 m to 4 m thick, with argillic and cambic soil morphologies in the upper 1 m of recognized units. The upper contact of Facies D sediments is truncated by aeolian erosion and buried by facies A and B sediments (Figs. 2 and 3).

Pleistocene lacustrine deposits, including tufa, have been identified previously intercalated within the Monahans's aeolian stratigraphy and penecontemporaneous with megafauna remains, including mammoth, mastodon and horse (Green et al., 1961). Extensive Pleistocene lacustrine deposits, of paleo-Lake Lomax, with associated molluscan fauna have also been reported from immediately eastward, in southwest Howard County and associated with wetter conditions during the late Pleistocene (Frye and Leonard, 1968; Cano-Garcia, 1999). Consistent with these previous studies the Quarry Site, an excavation for road gravel, ~ 3.5 km west of the Monahans dune field (Figs. 1b and 3; Table 1), revealed in near vertical walls calcareous deposits with extensive shallow-water, biogenic, and primary sedimentary structures (Wiest et al., 2020). Specifically, this site revealed calcereous rich sands with simple, subvertical shafts with slightly enlarged termal chambers (Camborygma isp.) that penetrate and crosscut the basal aeolian sand. These traces are analogous to modern crayfish burrows and indicate the position of the paleowater table (e.g., 1993; Hasiotis and Honey, 2000; Hembree and Swaninger, 2018; Lukens et al. 2019). The uppermost unit exhibits algal-induced microfabric with domal mounds and numerous in situ polygonal mud cracks, reflecting periodic drying at the edge of a water body (Wiest et al., 2020).

2.0 Methods

2.1 OSL dating of quartz grains from Geoprobe cores and stratigraphic sections

The targets for OSL-SAR and TT-OSL dating are quartz grains from seven Geoprobe direct-

push continuous cores (MON17-01, -03, -07, and -08, MON18-17, MON19-30, and -31) taken from the vicinity of the Monahans dune field and for one stratigraphic section in a nearby quarry (Fig. 1b; Table 1). The Geoprobe Macro-Core® (MC7, 7.0 cm diameter) sample tubes were "crown" cut, opening about 20% of the circumference to maximize the preservation of sunlight-shielded sediments for OSL dating and other analyses. These cores were studied extensively, noting Munsell colors, sedimentologic and pedologic features, particle size changes, and lithology-based unit boundaries. Subsequently, the cores were sampled at varying intervals between 2 and 20 cm for granulometry (using a Malvern 2000 Particle Size Analyzer) and carbonate content (gasometric method), with finer sampling intervals for increased discernment of unit contacts and the properties of buried soils. After pedo-sedimentary analyses, pedogenically-unaltered sediments were sampled for OSL dating to constrain aeolian depositional events and ensuing periods of soil formation (Fig. 3). The stratigraphy of the Quarry Site was documented, and blocks of sediments were extracted, which were sampled in the laboratory for OSL dating (Wiest et al., 2020).

OSL samples were extracted from the sediment blocks and light-shielded center of the cores within the Geoluminescence Dating Research Laboratory at Baylor University under sodium-vapor illumination (peak emission 589 nm), conditions in which mineral luminescence is preserved (Spooner et al., 2000). The extracted quartz-rich sediments (87-95%) were prepared to isolate a pure (> 99%) fraction of quartz grains of specific grain size as outlined in Marin et al. (2021). Feldspar grains are rare in Monahan sediments, accounting for < 2% of the grains, necessitating the use of TT-OSL on quartz grains for dating sediments > 75 ka old. Specific analytical details for SAR-OSL and TT-OSL are provided in Appendix 2.

2.2 Thermal Transfer Optically Stimulated Luminescence (TT-OSL) Dating

A common age limitation for single aliquot regeneration (SAR) protocols for dating quartz is 200 to 50 ka, which mostly reflects dose saturation, a plateau in equivalent dose (D_e) between 200 and 100 grays (Appendix 2). In contrast, TT-OSL protocols for dating quartz grains can yield D_e values up to 1000 grays (Duller and Wintle, 2012), with near apparent linear ingrowth of luminescence, (Appendix 2; Fig. 6) with corresponding ages from ca. 500 to 100 ka or older, with this variability in apparent age limit reflecting partially, variations in the environmental dose rate (D_r) . Ideally, this quartz-based geochronometer exhibits sufficient thermal stability of accumulated charge within the crystal lattice, with trap lifetimes >10^{6.1} years at a burial temperature of 10° C (e.g., Wang et al., 2006; 2007; Pagonis et al., 2008; Timar-Gabor and Wintle, 2013; Zander and Hilgers, 2013; Arnold et al., 2015; Faerstein et al., 2018). A potential limiting factor on the age range of TT-OSL is the possible thermal instability of trapped charge evaluated as the retention lifetime (e.g., Aitken, 1998 p. 199; Li and Li, 2006; Adamiec et al., 2010; Shen et al., 2011; Faerstein et al., 2018). The trap retention lifetime should be at least tentimes the measured age to obviate an underestimation effect of > 5% (e.g., Aitken, 1998, p. 200; Adamiec et al., 2010; Shen et al., 2011; Faershtein et al., 2018). Calculations using isothermal decay, assorted heating schemes, and modeling indicate variable lifetimes for the TT-OSL signal in quartz of ~0.2, 3.2, 3.9, 4.5, or 100's Ma at 10° C (e.g., Li and Li, 2006; Adamiec et al., 2010; Shen et al., 2011; Brown and Forman, 2012; Chapot et al., 2016; Faershtein et al., 2018). Recent reviews underscore that TT-OSL ages up to ~1.15 Ma on aeolian, littoral, and fluvial deposits appear to be generally concordant with independent age control (Arnold et al., 2015; Bartz et al., 2019), which is at odds with robust calculations on quartz TT-OSL trap lifetimes (at 10° C) of

3.2 Ma for middle eastern quartz (Faershtein et al., 2018). We assert that additional chronologic tests of quartz TT-OSL dating are needed in comparison to robust OSL-SAR ages in undisputed aeolian stratigraphic context spanning the past 0.5 to 1 ma, such as in the Monahans, to further evaluate the veracity of TT-OSL as a geochronometer.

The TT-OSL emission is induced in the laboratory by exposure to an elevated temperature, usually 290° C, which results in transfer of time-indicative, deeply stored electrons (~1.57 eV) (e.g., Wang et al., 2007; Jacobs et al., 2011; Brown and Forman, 2012). This TT-OSL emission of quartz often shows resistance to solar resetting, compared to the OSL-SAR response (e.g., Tsukamoto et al., 2008; Porat et al., 2009; Jacobs et al., 2011). Thus, TT-OSL is most suitable for well solar-reset sediments, like aeolian quartz grains from the Monahans dune field. Specifically, the TT-OSL signal is reset to a low definable level with days to months of sunlight exposure whereas, the corresponding OSL-SAR signal is depleted in seconds to minutes (e.g., Duller, 2008; Jacobs et al., 2011). The peak emissions for the TT-OSL signal are comparatively low at 10^2 to 10^4 photon counts/0.4s, with corresponding OSL-SAR emissions of 10^5 to 10^6 photon counts/0.4s. The resultant low photon output and signal-to-noise ratio, low sensitivity to laboratory irradiation and changing dose sensitivities with thermal transfer may lower the precision of D_e determinations (e.g., Pagonis et al., 2008; Brown and Forman, 2012).

2.3 Evaluation of the sensitivity for solar resetting of TT-OSL

The rate of solar resetting of the TT-OSL signal was evaluated in the laboratory for Monahans quartz grains to provide insights on the reduction of thermal-transferred luminescence with natural sunlight. Specifically, solar resetting experiments of quartz

extracts were evaluated for seven samples (BG4595, BG4563, BG4511, BG4571, BG4648, BG4996, and BG5021) from the seven cores studied (Fig. 4). These experiments were completed with exposure to UVA, UVB, and visible wavelengths at an intensity of 1000 W/m² from a Honle UVACUBE 400 solar simulator. This light intensity is about twice the average solar output at the Monahans dune field (31.6° N, 102.8° W). The quartz grains within the solar simulator were exposed to light at timed intervals of 0, 0.08, 0.25, 1, 4, 10, 24, 48, 100, 168, 264, 336, 600 h (see Fig. 4).

The residual D_e was measured to evaluate natural solar resetting for contemporary quartz from active dunes at the surface analogous to deeper aeolian strata sampled by Geoprobe cores. These modern grains were most likely exposed to sunlight for weeks to months and yielded an appropriate estimate of the residual for thermal-transfer luminescence (e.g., Arnold et al., 2018; Neudorf et al., 2019). The quartz grains were analyzed by OSL-SAR and TT-OSL protocols to yield apparent D_e values and evaluated the extent of solar resetting for modern analogous aeolian sands (Appendix 2).

3.0 Results

3.1 Resetting of TT-OSL by timed exposures from a solar simulator

There was a marked decrease in the normalized TT-OSL signal (L_x/T_x) after a few hours of light exposure from the Honle UVACUBE 400 solar simulator (Fig. 4). These quartz extracts showed a > 50% reduction of the natural signal within the first hour and a total of 80% reduction in the subsequent 8 h. This signal was further decreased to \geq 90% of the original natural emissions after 96 h of light exposure (Fig. 4). The Monahans quartz grains showed considerable variability in the duration of solar simulator exposure needed to deplete the TT-OSL emissions to

a negligible level (< 1% natural TT-OSL). For example, the luminescence of quartz grains for BG4595 was reduced to a low definable level after 24 h, whereas the corresponding luminescence of BG4571 was reduced to this level after \sim 480 h of sunlamp exposure. There was also apparent stratigraphic variability for the TT-OSL solar resetting of quartz grains. Quartz grains that yielded higher D_e values of > 209 Gy (BG4563, BG4571, BG4511, BG4996, BG5021) showed a higher percentage remnant signal (18 \pm 6%) after 48 h of solar resetting than of quartz grains with lower D_e values of <107 Gy (2 \pm 1%) (BG4595 and BG4648), though the sample size is small. However, the remnant signal for quartz grains after 90 h sunlamp exposure is relatively small < 5% (Fig. 4), which translates to \leq 0.5 standard deviation unit of the corresponding D_e .

The TT-OSL signals for the Monahans quartz grains showed greater sensitivity to solar resetting than quartz grains from other localities in the Northern Hemisphere (Fig. 5). Most other quartz grains exhibit a 90% reduction after weeks to months of light exposure, with Monahans quartz achieving this reduction in < 3 to 4 days (Fig. 4). However, the Monahans' grains show less sensitivity to solar resetting than aeolian quartz grains from one locality in southern Greece, with a 90% reduction in TT-OSL signal after an hour of exposure to natural sunlight (Athanassas and Zacharias, 2010) (Fig. 4).

Three modern analog samples (BG4866, BG4882, and BG5035) from the surface of active dunes, retrieved from tops of cores for MON18-17, MON17-01, and MON19-31 were tested to assess if ongoing aeolian processes fully solar reset the TT-OSL signal. Quartz extracts from contemporary aeolian sands returned OSL-SAR D_e values of $< 0.50 \pm 0.01$ Gy. Subsequently, TT-OSL analysis of these same quartz extracts yielded a statistically insignificant signal, well within background counts, yielding D_e values < 0.05 Gy. This near

naught result was similar to many well-solar-reset modern analogs (equivalent to 0 Gy at 2σ) measured by single-grain TT-OSL analyses of other aeolian sediments from north-central Spain (Arnold et al., 2014, 2018) and southern Australia (Neudorf et al., 2019). Thus, the solar resetting and modern analog data indicate that the TT-OSL inheritance of Monahans sand grains was indistinguishable from the background emissions and was well within the 0.5 σ errors for D_e determinations. Finally, residual tests on all dated quartz separates, post TT-OSL analysis yielded consistent values <0.5 Gy, another indicator of insignificant luminescence inheritance.

3.4 Equivalent dose determinations by TT-OSL and OSL-SAR on Monahans quartz grains

Quartz grains from the Monahans by OSL-SAR show dose saturation, as modeled by an exponential function, $(2D_{0;})$ between 100 and 200 grays (Appendix 2; Fig. 6), which is equivalent to 130 to 260 ka, depending on the environmental dose rate (Table 2). TT-OSL analysis of the deepest and oldest quartz grains yielded apparent D_e between 300 and 370 Gy with low order polynomial equations modeling regenerative growth constrained up to 600 to 700 Gy (Appendix 2). Exponential models indicate apparent dose saturation at 1400 to 1600 Gy, equivalent to ca. 2 ma, assuming an D_r of 0.75 Gy/ka. This hypothesized upper limit needs to be further tested by dating aeolian sand in the proximity of the Lava Creek B (0.631 ma) and Guaje Ash (1.61 Ma) or geomagnetic polarity events such as, the Brunhes-Matuyama geomagnetic polarity reversal event (0.781 Ma) (e.g., Gustavson, 1996; Stine et al., 2020).

Five quartz separates (BG4515, BG4595, BG4648, BG4647, and BG4596) were dated in parallel by OSL-SAR and TT-OSL protocols to evaluate the reproducibility of ages using these two different geochronometers (Fig. 7). These quartz grains were dated by both methods because of the low environmental dose rate (0.43 to 0.71 mGy/ka), suspected age range between 50 and

250 ka. Also, the OSL-SAR regenerative growth was below the saturation dose and with photon emissions at least three times background values for statistically significant TT-OSL analyses. Quartz grains from the SHP with a D_e < 45 Gy may exhibit a low signal-to-noise response (< 3:1), which may confound D_e calculations by TT-OSL for sediments ca. 50 to 75 ka old. These results indicate internal consistency between the TT-OSL and OSL-SAR ages for the Monahans dune field for the tested D_e range of ~46 to 145 Gy, with this concordance indicating that the TT-OSL component(s) was apparently well solar reset and with thermal stability at least up to 145 Gy, equivalent to ca. 250 ka (Fig. 7).

3.5 Sedimentary sequence for the Monahans dune field

A total of > 88 m of core length for seven core was examined for this study (Fig 3) with the dominant occurrence of well sorted aeolian sands, often with lesser amounts of silt (0-30%) and common pedogenesis (Appendix 2). The identification and correlation of stratigraphic units amongst cores in this study is hampered because of the non-unique sedimentary signature of this sand-dominated aeolian environment, subsequent pedogenic imprints, and numerous erosional hiatuses (Fig. 3). Thus, to effectively decipher aeolian depositional sequences OSL dating of quartz grains is a formative approach, which provide close interval ages to reconstruct a chronostratigraphy of aeolian depositional phases (ADP), though incomplete, spanning 10²-to-10⁴-year timescales, which we adopt in this analysis (Tripaldi and Forman, 2016). A noticeable feature of the Monahans stratigraphic record is that no two cores fully replicate another, though there are broad stratigraphic similarities amongst cores (Fig. 3). Most cores show 1-to-9-m below the surface a complex of welded, buried soils of facies C and D at least 2 m thick (Figs. 2 and 3), often with stage 2 to 4 carbonate soil morphologies. Quartz grains from underlying and

contained sediment from this pedo-complex yielded TT-OSL ages between ca. 105 and 560 ka, the oldest recognized sediments. This lower, oldest sedimentary sequence is highly incomplete with multiple erosional hiatus most often at the boundary between buried soils and the overlying aeolian sand. Overtop this pedo-complex are the youngest sediments, <65 ka often showing less pedogenic alterations, mostly composed of facies A, B, and D type sediments (Fig. 3). The age of surface sediments around the Monahans range from ca. 70 years to 20 ka, reflecting a temporal mosaic of aeolian erosion, exposure, and deposition in this sand sheet environment proximal to the Monahans dune field.

4.0 Discussion:

4.1 Timing of Aeolian Depositional Periods (ADP)

Questions remain on the accuracy of TT-OSL dating particularly with a $D_e > 300$ Gy (e.g., Faershtein et al., 2018). The concordance between SAR-OSL and TT-OSL ages up to 145 Gy is supportive of the utility of TT-OSL dating in the Monahans dune field context. The low dose rate of 0.4 to 1.4 mGy/yr for the Monahans aeolian sand may also limit the upper temporal range, but the selection of aliquots with fast ratios > 2 may enhance temporal sensitivity (Faershtein et al., 2018). The oldest ages with a D_e between 300 and 370 Gy may be minimum estimates. These results indicate the need for thermal stability studies of the TT-OSL source trap for the Monahans quartz grains (e.g., Faershtein et al., 2018), and/or the application of other luminescence dating approaches, such as violet stimulation (e.g., Ankjærgaard, 2019), and U-series dating on dense soil carbonate to test these ages (e.g., Durand et al., 2016). We view the oldest ages of ca. 550 ka as a new chronologic hypothesis for subsequent testing.

The total of sixty-one OSL ages on seven >7-m-long Geoprobe cores, and one stratigraphic

section (Fig. 3) provides improved chronologic definition on past, preserved aeolian depositional periods (ADP; Forman et al., 2014; Tripaldi and Forman, 2016), often bounded by buried soils. Also, bounding luminescence ages for buried carbonate soils yield age differences of 10³ to 10⁴ years providing maximum limiting age estimates on depositional and erosional hiatuses, and on periods of landscape stability. TT-OSL dating provided improved definition on ADPs > 60 ka ago, with SAR-OSL dating yielding ages for quartz extracts < 100 ka. These two luminescence dating approaches on the same quartz extracts provide concordant ages overlapping at one sigma errors for ages between 50 and 250 ka; yielding added confidence in the resolved depositional chronology for the past ca. 250 ka (Fig. 7).

The recognition of aeolian depositional periods was assisted through a finite mixture modeling (Galbraith and Roberts, 2012; Liang and Forman, 2019) of the forty finite OSL ages associated with this study (Table 2; Fig. 8). The oldest preserved ADP defined solely by TT-OSL ages on quartz grains is at 510 ± 35 ka (n= 7). This appears to be a significant episode of aeolian activity with over 5-m-thickness of aeolian sand (Facies B or D) found in three cores (MON17-07, 19-30 and 19-31), reflecting dune-like environments and interrupted in places by noticeable soil development, with cambic horizons (Fig. 3). This period of aeolian deposition generally corresponds with Marine Oxygen Isotopic Stages (MIS) 14 and 13 (Fig. 8), when global sea level was -20 to -80 m, possibly associated with an intermediate configuration of North American ice sheets (Past Interglacial Working Group of Pages, 2016; Batchelor et al., 2019; Rohling et al., 2021). There were two succeeding aeolian deposits recognized by sole TT-OSL ages of 444,250 \pm 26,760 yr (BG4563TT) and 347,680 \pm 21,210 yr (BG4760TT) in core MON07-03 and at the Quarry site respectively, that are < 2 m thick and altered heavily by

secondary pedogenic carbonate (Fig. 3). Aeolian sediments which yielded an IRSL age of 347 ± 40 ka have also been recognized in BWD formation to the north, near Lubbock, TX (Hall and Goble, 2020). These aeolian depositional events may have occurred during *sensu lato* glacial MIS 12 and 10, respectively, considering errors in ages (Fig. 8). Northern Hemisphere ice sheets during these intervals were near Last Glacial Maximum (LGM) size and associated with global sea level of < -60 m (Past Interglacial Working Group of Pages, 2016; Batchelor et al., 2019; Rohling et al., 2021).

The Quarry Site, 3.5 km west of the Monahans dune field (Wiest et al., 2020), revealed evidence for wetter conditions in the past 250 ka than today (Fig. 3). The most compelling evidence is the stratigraphic presence of crayfish-burrow-like *Camborygma*, domal structures with algal-induced microfabric, and paleo-mud cracks dated by bounding TT-OSL ages of 233,150 ± 14,540 yr (BG4765TT) and 196,420 ± 10,910 yr (BG4761TT). This wet period may have occurred broadly during interglacial MIS 7 (Fig. 8) and may reflect added precipitation associated with a thermally driven increase in advective moisture from the Gulf of Mexico (cf. Insel and Berkelhammer, 2021). These near-shore palustrine deposits are correlative to a tripartite stack of carbonate-rich paleosols in core MON18-17 that span from ca. 255 ka to 188 ka and a dual sequence of carbonate-rich paleosols dated between 251 ka and 107 ka in core MON17-01 (Fig. 3), indicating landscape stability of the Monahan dunes during this wet period, ca. 235 to 195 ka.

Aeolian deposits from the last interglacial (MIS 5) ca. 135 to 75 ka (Fig. 8) are uncommon in the study area. There are just two minor occurrences of sediments each \sim 1 m thick, with strong pedogenic overprinting as cambic and argillic horizons, with C horizon sediments that yielded OSL ages of 129,180 \pm 8,810 yr (BG4993) and 96,050 \pm 10,120 yr (BG5003), with

truncated upper contacts. The emplacement of sand sheet deposits post ca. 95 ka truncated these buried soils and is consistent with the timing of deposition of the Mescalero sand sheet at ~90 to 70 ka in adjacent New Mexico which buries the well-developed Mescalero soil, with stage 3 to 4 soil carbonate morphologies (Hall and Goble, 2006, 2015; Hall et al., 2010). Recent modeling of last interglacial climate indicates that there may have been a precipitation dipole with drier conditions in Arizona, and wetter conditions in eastern New Mexico and West Texas ca. 130-125 ka, with an increase in thermally driven advective moisture from the Gulf of Mexico (Insel and Berkelhammer, 2021). The scantly preserved aeolian deposits and well developed paleosols during MIS5 indicate net modest aeolian deposition (and preservation) occurred during one of warmest interglacial in the past 500 ka (Past Interglacial Working Group of Pages, 2016; Rohling et al., 2021), perhaps reflecting more mesic conditions than the 21st century (Insel and Berkelhammer, 2021).

There is persistent evidence in cores MON17-01, 17-03, 17-08, 18-17, and 19-31 of 2 to 5 m accumulation and preservation of aeolian sand (Facies A and B) deposited ca. 65 to 30 ka ago (Fig. 3), equivalent with MIS 4 and 3. Speleothem records from Missouri indicate that this is a period of cooling and drying in the mid-continental US (Dorale et al., 1998) with the dominance of grassland on the eastern Great Plains (Baker et al., 2009), punctuated by possible droughts at ca. 66 ka in east Texas, associated with the demise of large nursery herd (s) of mammoths (Wiest et al., 2016; 2017). Clumped isotopic analyses on pedogenic carbonate from eastern Wyoming indicate a shift in mean precipitation-bearing circulation in mid-continental U.S. from zonal to meridional ca. 70 to 55 ka, with expansion of the Laurentide ice sheet and drying of interior North America

(Oerter et al., 2016).

The aeolian depositional record for the LGM, ca. 25 to 15 ka is discontinuous with <1 to 2 m thick of recognized strata in five out of six cores (Fig. 4). These sand sheet-type deposits are often reworked BWD equivalent sediments (Facies B sands) and show a noticeable pedogenic overprinting of carbonate and cambic horizons, indicating stable landscape conditions (Fig. 3). The presence of pluvial Lake King in a closed basin in the Rio Grande drainage immediately west of the Monahans Dune Field that formed ca. 25 to 16 ka ago, with at least four distinct high stands (Wilkens and Currey, 1997; Wilkens, 1997) indicates appreciably wetter conditions late during the LGM. These ameliorated conditions may have persisted periodically past the Younger Dryas Chronozone (ca. 12.9 to 11.5 ka) with evidence of a stable landscape surface with appreciable soil development (Tubb soil) in a small satellite dune field to the southwest of the Monahans dune field (Meltzer et al., 2006) and within the Monahans dune field (Hofman et al., 1990). Cores MON17-01, MON17-31 and MON18-17 from the Monahans Dune Field may have identified a correlative paleosol, buried by 1.5 to 4 m of aeolian sand ca. 13 and 10 ka ago, indicating renewed aeolian activity and drying into the Holocene.

Conclusions

Stratigraphic analyses of seven Geoprobe cores and one section associated with the Monahans dune field, West Texas with sixty-one associated OSL ages by single aliquot regeneration and thermal transfer approaches provide new data for deciphering the preserved record of aeolian deposition and environmental changes spanning the past ca. 500 ka (Fig. 8). The two OSL dating protocols on the same quartz extracts yielded concordant ages between 50 and 250 ka, providing added confidence in the chronology, though the oldest ages of 500 to 550

ka may be minimum estimates. This record revealed that each core has limited chronostratigraphic commonalities reflecting biases of sediment preservation, associated with dominance of erosional processes at this dune field margin and the presence of erosion resistant carbonate and argillic buried soils. The OSL ages in concert with sedimentologic features, granulometry, finite mixture modeling of ages revealed at least four, broad, preserved aeolian depositional periods at ca. 545 to 475, 300 to 260, 67 to 30, and post 16 ka. However, there may be two interceding aeolian depositional periods, though just recognized by sole TT-OSL ages of $444,250 \pm 26,760$ yr (BG4563TT) and $347,680 \pm 21,210$ yr (BG4760TT) in core MON07-03 and at the Quarry Site respectively, that are < 2 m thick and altered heavily by secondary pedogenic carbonate (Fig. 3). The greatest preserved stratigraphic thicknesses (3-6 m) of aeolian sand are for periods 545 to 475 ka, 67 to 30 ka ago and the past 16 ka. These thickest preserved aeolian deposits occurred mostly during transitional climate periods, e.g., contemporaneous with stadials, when the Laurentide ice sheet was 40 to 80% of the last glacial maximum volume, and precipitation-bearing zonal circulation was shifted northward (Schmidt and Hertzberg, 2011; Dalton et al., 2022). In contrast, relatively moist periods persisted as indicated by the formation of pluvial lakes in the region during interglacial MIS 7, ca. 235 to 195 ka, and during the last deglacial period MIS 2, ca. 25 to 16 ka (Fig. 8), as Lake King, straddling the upper Rio Grande watershed (Wilkens and Currey, 1997). These wetter periods are correlative with modest (< 2 m thick) aeolian deposition overprinted by pedogenesis forming > 0.5 m thick carbonate and argillic dominated soils, often welded together. This chronostratigraphic study underscores that there may be multiple climatic states, during glacials and interglacials, associated with wetter conditions. In turn, drier

conditions with dune movement and aeolian erosion occurred preferentially during intermediate climate states, such as stadials with advance and retreat phases of the Laurentide ice sheet, during the past ca. 500 ka, which modulated zonal precipitation (Schmidt and Hertzberg, 2011; Dalton et al., 2022).

Acknowledgements

This research was supported initially through grants from the National Science

Foundation (Award GSS-1660230) and the National Geographic Society (#9990-16). Vital support for graduate students and post-doctoral scholar, and unfettered access to the Monahans's property was provided by the generosity of Atlas Sand Company, LLC in Austin, TX. The logistical assistance of many employees at the Monahans Plant was pivotal; thanks for all the cold water, a cool place to rest, and out-towing from sand traps. Assistance in obtaining Geoprobe cores is much appreciated from the able efforts of Peng Liang, Shengli Yang, Don Esker and Yongui Song. Many thanks go to Gary Kocurek for opening our eyes to the wonders of the Monahans and later discussions on stratigraphic incompleteness. Fieldwork with Mark Sweeney was the source of ideas on contemporary and past aeolian processes. Insightful review comments by Jill Onken are appreciated. The detail comments of two anonymous reviewers and editors were helpful in strengthening the presentation of this paper. Each study reveals partially, and all shortcomings are solely the responsibility of the authors.

References

- Adamiec, G., Duller, G.A.T., Roberts, H.M., Wintle, A.G., 2010. Improving the TT-OSL SAR protocol through source trap characterization. Radiat. Meas. 45(7), 768-777.
- Aitken, M.J., 1998. An Introduction to Optical Dating: The Dating of Quaternary Sediments by the Use of Photon-Stimulated Luminescence, Oxford Science Publications.
- Ankjærgaard, C., 2019. Exploring multiple-aliquot methods for quartz violet stimulated luminescence dating. Quat. Geochron. 51, 99-109.
- Arnold, L. J., Demuro, M., Parés, J. M., Arsuaga, J. L., Aranburu, A., Bermúdez de Castro, J.
 M., Carbonell, E., 2014. Luminescence dating and palaeomagnetic age constraint on hominins from Sima de los Huesos, Atapuerca, Spain. J. Hum. Evol. 67, 85–107.
- Arnold, L.J., Demuro, M., Pares, J.M., Perez-Gonzalez, A., Arsuaga, J. L., de Castro, J. M. B., Carbonell, E., 2015. Evaluating the suitability of extended-range luminescence dating techniques over early and Middle Pleistocene timescales: Published datasets and case studies from Atapuerca, Spain. Quat. Int., 389, 167-190.
- Arnold, L. J., Demuro, M., Spooner, N. A., Prideaux, G. J., McDowell, M. C., Camens, A. B.,
 Reed, E. H., Pares, J. M., Arsuaga, J. L., de Castro, J. M. B., Carbonell, E., 2018. Single-grain
 TT-OSL bleaching characteristics: Insights from modern analogues and OSL dating
 comparisons. Quat. Geochron., 49, 45-51.
- Athanassas, C., Zacharias, N., 2010. Recuperated-OSL dating of quartz from Aegean (South Greece) raised Pleistocene marine sediments: current results. Quat. Geochron. 5, 65–75.
- Baird, H. 2015. Assessing Pleistocene climate on the Southern High Plains through geochemical and physical characteristics of paleosols archived in the Blackwater Draw Formation, MSc. Thesis, Dept. of Geology, Texas Tech University, Lubbock, TX, 199 pp.

- Baker, R.G., Bettis, E.A., III, Mandel, R.D., Dorale, J.A., Fredlund, G.G., 2009. Mid-Wisconsinan Environments on the eastern Great Plains. Quat. Sci. Revs. 28, 873-889.
- Bartz, M., Arnold, L.J., Demuro, M., Duval, M., King, G. E., Rixhon, G., Posada, C. A., Pares, J.
 M., Bruckner, H., 2019. Single-grain TT-OSL dating results confirm an Early Pleistocene age for the lower Moulouya River deposits (NE Morocco). Quat. Geochron., 49, 138-145.
- Batchelor, C. L., Margold, M., Krapp, M., Murton, D. K., Dalton, A. S., Gibbard, P. L., Stokes,C. R., Murton, J. B., Manica, A., 2019. The configuration of Northern Hemisphere ice sheetsthrough the Quaternary. Nature Comm., 10 (3713).
- Birkeland, P.W., 1999. Soils and Geomorphology, 3rd edition. Oxford University Press, New York, 430 pp.
- Brown, N. D., Forman, S. L., 2012. Evaluating a SAR TT-OSL protocol for dating fine-grained quartz within Late Pleistocene loess deposits in the Missouri and Mississippi river valleys, United States. Quat. Geochron., 12, 87-97.
- Cano-Garcia, M. A., 1999. Soil-geomorphic relationships in the ancient Lake Lomax Basin, Southern High Plains. Ph.D. Dissertation, Dept. of Agronomy, Texas Tech University, Lubbock, TX, 188 pp.
- Carlisle, W. J., Marrs, R. W., 1982. Eolian features of the Southern High Plains and their relationship to windflow patterns, in Marrs, R. W., and Kolm, K. E., eds., Interpretation of windflow characteristics from eolian landforms: Geol. Soc. Amer. Special Paper 192, 89-105.
- Chapot, M. S., Roberts, H. M., Duller, G. A. T., Lai, Z. P., 2016. Natural and laboratory TT-OSL dose response curves: Testing the lifetime of the TT-OSL signal in nature. Rad. Meas. 85, 41-50.

- Cosgrove, G.I.E., Colombera, L., Mountney, N.P., 2022. Eolian stratigraphic record of environmental change through geological time. Geology 50, 289-294.
- Dalton, A.S., Stokes, C. R., Batchelor, C. L., 2022. Evolution of the Laurentide and Innuitian ice sheets prior to the Last Glacial Maximum (115 ka to 25 ka). Earth Sci. Rev. 224, 103875.
- Dorale, J. A., Edwards, R. L., Ito, E., Gonzalez, L. A., 1998. Climate and vegetation history of the midcontinent from 75 to 25 ka: A speleothem record from Crevice Cave, Missouri, USA. Science 282, 1871-1874.
- Duller, G. A. T., 2008. Single-grain optical dating of Quaternary sediments: why aliquot size matters in luminescence dating. Boreas, 37(4), 589-612.
- Duller, G. A. T., Wintle, A. G., 2012. A review of the thermally transferred optically stimulated luminescence signal from quartz for dating sediments. Quat. Geochron. 7(1), 6-20.
- Durand, N., Hamelin, B., Deschamps, P., Gunnell, Y., Curmi, P., 2016. Systematics of U-Th disequilibrium in calcrete profiles: Lessons from southwest India. Chem. Geol. 446, 54-69.
- Elderfield, H., Ferretti, P., Greaves, M., Crowhurst, S., McCave, I.N., Hodell, D., Piotrowski, A.M., 2012. Evolution of Ocean Temperature and Ice Volume Through the Mid-Pleistocene Climate Transition. Science 337, 704-709.
- Faershtein, G., Porat, N., Matmon, A., 2018. Natural saturation of OSL and TT-OSL signals of quartz grains from Nilotic origin. Quat. Geochron. 49, 10.1016.
- Forman, S.L., Oglesby, R., Webb, R.S., 2001. Temporal and spatial patterns of Holocene dune activity on the Great Plains of North America: megadroughts and climate links. Glob. Planet. Change 29(1-2), 1-29.
- Forman, S. L., Tripaldi, A. Ciccioli, P. L., 2014. Sand sheet deposition in the San Luis paleodune field, western Argentina as an indicator of a semi-arid environment through the Holocene.

27.

- Paleogeog., Paleoclimat., Paleoecol. 411, 122-135.
- Forman, S. L., Wiest, L. A., Mayhack, C., Tew, V., Liang, P., Wu, Z., Money, G., 2019.

 Quaternary Geology and Geomorphology Division Farouk El-Baz Award for Desert

 Research: Fourth Dimensional Understanding of Late Pleistocene Aeolian Depositional

 Environments for the Monahans Dune Field, Texas USA, Geol. Soc. Amer. Annual Meeting.

 Phoenix, AZ, DOI:10.1130/abs/2019AM-337344.
- Frye, J. C., Leonard, A. B., 1968. Late Pleistocene Lake Lomax in western Texas, in Means of correlation of Quaternary successions, Proc. VII Congress International Assoc. for Quaternary Research (R. B. Morrison and H. E. Wright, eds.): University of Utah Press, v. 8, p. 519-534 Galbraith, R. F., Roberts, R. G., 2012. Statistical aspects of equivalent dose and error calculation and display in OSL dating. An overview and some recommendations. Quat. Geochron. 11, 1-
- Green, G.E., 1961. The Monahans Dunes Area, in: Wendorf, F. (Ed.), Paleoecology of the Llano Estacado. The Museum of New Mexico Press, Sante Fe New Mexico, Fort Burgwin Research Center Report 1, pp. 22-47.
- Gustavson, T. C., 1996. Fluvial and Eolian Depositional Systems, Paleosols, and Paleoclimate of the Late Cenozoic Ogallala and Blackwater Draw Formations, Southern High Plains, Texas and New Mexico: The University of Texas at Austin, Bureau of Economic Geology, Report of Investigations 239.
- Gustavson, T. C., Holliday, V. T., 1999. Eolian sedimentation and soil development on a semiarid to subhumid grassland, Tertiary Ogallala and Quaternary Blackwater Draw Formations, Texas and New Mexico High Plains. J. of Sed. Res. 69(3), 622-634.
- Halfen, A. F., Johnson, W. C., 2013. A review of Great Plains dune field chronologies. Aeolian

- Res. 10, 135-160.
- Hall, S. A., Goble, R. J., 2006. Geomorphology, stratigraphy, and luminescence age of the Mescalero Sands, southeastern New Mexico. New Mexico Geological Society 57th Annual Fall Field Conference Guidebook, 297-310.
- Hall, S.A., Goble, R.J., 2012. Berino Paleosol, Late Pleistocene Argillic Soil Development on the Mescalero Sand Sheet in New Mexico. J. Geol. 120, 333-345.
- Hall, S. A., Goble, R. J., 2015. OSL age and stratigraphy of the Strauss sand sheet in New Mexico, USA. Geomorphology 241, 42-54.
- Hall, S.A., Goble, R. J., 2020. Middle Pleistocene IRSL age of the upper Blackwater Draw Formation, Southern High Plains, Texas and New Mexico, USA. New Mexico Geology 42(1), 31-38.
- Hall, S. A., Miller, J., Myles R., Goble, R. J., 2010. Geochronology of the Bolson sand sheet, New Mexico and Texas, and its archeological significance. Bull. Geol. Soc. Amer. 122(11/12), 1950-1967.
- Hasiotis, S. T., Mitchell, C. E., A comparison of crayfish burrow morphologies: Triassic and Holocene fossil, paleo- and neo-ichnological evidence, and the identification of their burrowing signatures Ichnos 2, 291-314.
- Hasiotis, S. T., Honey, J. G., 2000. Paleohydrologic and stratigraphic significance of crayfish burrows in continental deposits: Examples from several Paleocene Laramide basins in the Rocky Mountains. J. Sed. Res. 70(1), 127-139.
- Hembree, D. I., Swaninger, E. S., 2018. Large Camborygma isp in fluvial deposits of the Lower Permian (Asselian) Dunkard Group, southeastern Ohio, USA. Palaeogeogr. Palaeoclimatol. Palaeoecol. 491, 137-151.

- Hofman, J. L., Amick, D. S., Rose, R. O., 1990. Shifting sands: a Folsom-Midland assemblage from a campsite in western Texas. Plains Anthropologist 35, 221–253.
- Holliday, V.T., 1989. The Blackwater Draw Formation (Quaternary): A 1.4-plus-m.y. record of eolian sedimentation and soil formation on the Southern High Plains. Bull. Geol. Soc. Amer. 101, 1598-1607.
- Holliday, V. T., 1995. Stratigraphy and Paleoenvironments of Late Quaternary Valley Fills on the Southern High Plains: Geol. Soc. Amer. Memoir 186, 136 pp.
- Holliday, V. T., Mayer, J. H., Fredlund, G. G., 2008. Late Quaternary sedimentology and geochronology of small playas on the Southern High Plains, Texas and New Mexico, USA. Quat. Res. 70(1), 11-25.
- Huffington, R. M., Albritton, jr., C. C., 1941. Quaternary Sands on the Southern High Plains of Western Texas. Am J. Sci. 239, 325-338.
- Insel, N., Berkelhammer, M., 2021. The influence of orbital parameters on the North American Monsoon system during the Last Interglacial Period. J. of Quat. Sci., 36(4), 638-648.
- Izett, G. A., Wilcox, R. E., Borchart, G. A., 1972. Correlation of a volcanic ash bed in Pleistocene deposits near Mt. Blanco, Texas, with the Guaje pumice bed of the Jemez Mountains, New Mexico. Quat. Res. 2, 554-578.
- Izett, G. A., Obradovich, J. D., 1994. 40Ar/39Ar age constraints for the Jaramillo Normal Subchron and the Matuyama-Brunhes geomagnetic boundary. J. Geophys. Res., 99(B2), 2925-2934.
- Jacobs, Z., Roberts, R. G., Lachlan, T. J., Karkanas, P., Marean, C. W., Roberts, D. L., 2011.
 Development of the SAR TT-OSL procedure for dating Middle Pleistocene dune and shallow
 marine deposits along the Southern Cape coast of South Africa. Quat. Geochronol., 6(5), 491-

- Kemp, R. A., 2001. Pedogenic modification of loess: Significance for paleoclimatic reconstructions. Earth Sci. Rev., 54, 145-156.
- Li, B., Li, S. H., 2006. Studies of thermal stability of charges associated with thermal transfer of OSL from quartz: Journal of Physics D-Applied Physics 39(14), 2941-2949.
- Lukens, W., Fox, D., Snell, K., Wiest, L., Layzell, A., Uno, K., Polissar, P., Martin, R., Fox-Dobbs, K., Peláez-Campomanes, P., 2019. Pliocene Paleoenvironments in the Meade Basin, Southwest Kansas, U.S.A. J. Sediment. Res. 89, 416-439.
- Liang, P., Forman, S. L., 2019. LDAC: An Excel-based program for luminescence equivalent dose and burial age calculations. Ancient TL 37 (2), 21-40.
- Matthews, N. E., Vazquez, J. A., Calvert, A. T., 2015. Age of the Lava Creek supercruption and magma chamber assembly at Yellowstone based on ⁴⁰Ar/³⁹Ar and U-Pb dating of sanidine and zircon crystals. Geochem. Geophys. Geosyst. 16, 2508–2528.
- Marin, L. C., Forman, S. L., Todd, V. T., Mayhack, C., Gonzalez, A., Liang, P., 2021. Isolation of quartz grains for optically stimulated luminescence (OSL) dating of Quaternary sediments for paleoenvironmental research. J. Vis. Exp. (174), e62706, doi:10.3791/62706205.
- Mayhack, C., 2021. Late Quaternary Sedimentary Architecture and Depositional History of the Monahans Dune Field, Winkler County, TX. Baylor University, Geoscience, MSc Thesis, 40 pp.
- McKean, R. L. S., Goble, R. J., Mason, J. B., Swinehart, J. B., Loope, D. B., 2015. Temporal and spatial variability in dune reactivation across the Nebraska Sand Hills, USA. Holocene 25(3), 523-535.
- Meltzer, D. J., Seebach, J. D., Byerly, R. M. 2006. The Hot Tubb Folsom-Midland Site (41 CR

- 10), Texas. Plains Anthropologist 51 (198), 157-184.
- Muhs, D.R., Holliday, V.T., 1995. Evidence of Active Dune Sand on the Great-Plains in the 19th-Century from Accounts of Early Explorers. Quat. Res. 43, 198-208.
- Muhs, D. R., Holliday, V. T., 2001. Origin of late quaternary dune fields on the Southern High Plains of Texas and New Mexico. Bull. Geol. Soc. Amer. 113(1), 75-87.
- Muhs, D. R., Reynolds, R. L., Been, J., Skipp, G., 2003. Eolian sand transport pathways in the southwestern United States: Importance of the Colorado River and local sources. Quat. Int. 104, 3-18.
- Neudorf, C. M., Lian, O. B., McIntosh, P. D., Gingerich, T. B., Augustinus, P. C., 2019.
- Investigation into the OSL and TT-OSL signal characteristics of ancient (> 100 ka) Tasmanian aeolian quartz and its utility as a geochronometer for understanding long-term climate-driven landscape change. Quat. Geochron., 53, 101005.
- Oerter, E.J., Sharp, W.D., Oster, J.L., Ebeling, A., Valley, J.W., Kozdon, R., Orland, I.J., Hellstrom, J., Woodhead, J.D., Hergt, J.M., Chadwick, O.A., Amundson, R., 2016. Pedothem carbonates reveal anomalous North American atmospheric circulation 70,000-55,000 years ago. P. Natl. Acad. Sci. 113, 919-924.
- Olson, C. G., Nettleton, W. D., 1998. Paleosols and the effects of alteration. Quat. Int., 51/52, 185-194.
- Pagonis, V., Wintle, A. G., Chen, R., Wang, X. L., 2008. A theoretical model for a new dating protocol for quartz based on thermally transferred OSL (TT-OSL). Rad. Meas. 43, 704-708.
- Past Interglacials Working Group of PAGES, 2016. Interglacials of the last 800,000 years. Rev. Geophys. 54, 162-219.
- Porat, N., Duller, G. A. T., Roberts, H. M., Wintle, A. G., 2009. A simplified SAR protocol for

- TT-OSL. Rad. Meas. 44(5-6), 538-542.
- Rich, J., 2013. A 250,000-year record of lunette dune accumulation on the Southern High Plains, USA and implications for past climates. Quat. Sci. Revs. 62, 1-20.
- Rich, J., Stokes, S., 2001. Optical dating of geoarchaeologically significant sites from the Southern High Plains and South Texas, USA. Quat. Sci. Revs. 20, 949–959.
- Rich, J., Stokes, S., 2011. A 200,000-year record of late Quaternary Eolian sedimentation on the Southern High Plains and nearby Pecos River Valley, USA. Aeol. Res. 2(4), 221-240.
- Rohling, E. J., Yu, J., Heslop, D., Foster, G. L., Opdyke, B., Roberts, A. P., 2021. Sea level and deep-sea temperature reconstructions suggest quasi-stable states and critical transitions over the past 40 million years. Sci. Adv. 7, eabf5326.
- Ruhe, R. V., Olson, C.G., 1980. Soil welding. Soil Sci. 130:132-139.
- Schmidt, M., Hertzberg, J., 2011. Abrupt climate change during the last Ice Age. Nat. Educ. Know. 3(10), 11.
- Shen, Z. X., Mauz, B., Lang, A., 2011. Source-trap characterization of thermally transferred OSL in quartz. J. of Phys. D-Appl. 44(29), 12.
- Spooner, N. A., Questiaux, D. G., Aitken, M. J., 2000. The use of sodium lamps for low-intensity laboratory safe lighting for optical dating. Ancient TL 18, 45–49.
- Stauch, G., 2019. A conceptual model for the interpretation of aeolian sediments from a semiarid high-mountain environment since the late glacial. Quat. Res., 91, 24-34.
- Stine, J., Sweet, D. E., Geissman, J. W., Baird, H., and Ferguson, J. F., 2020, Climate and provenance variation across the mid-Pleistocene transition revealed through sedimentology, geochemistry, and rock magnetism of the Blackwater Draw Formation, Southern High Plains,

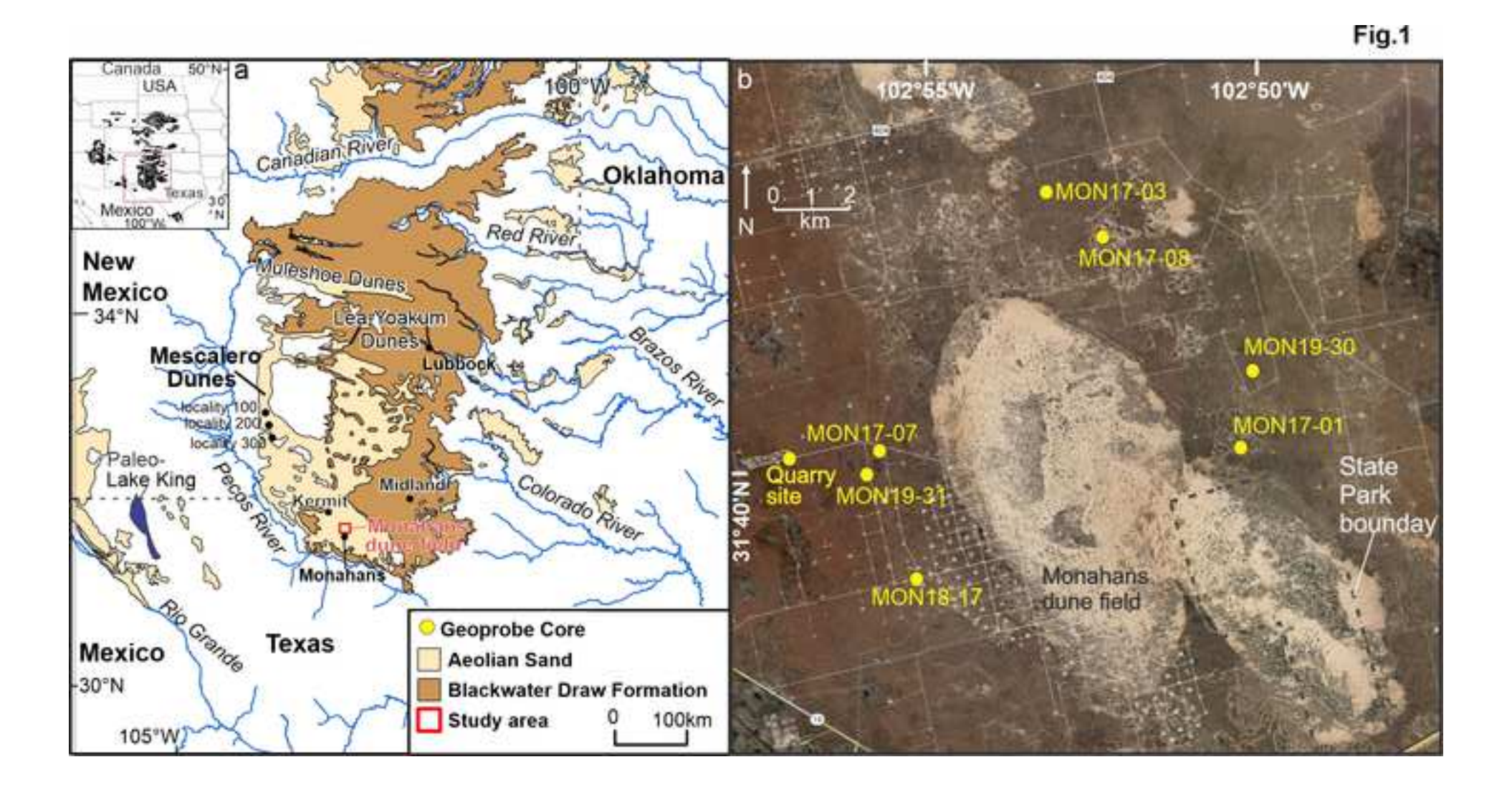
- Texas, USA, *in* Waitt, R. B., Thackray, G. D., and Gillespie, A. R., eds., Untangling the Quaternary Period: A Legacy of Stephen C. Porter: Geol. Soc. Amer. Spec. Paper 548.
- S. Stokes, H. E. Bray. 2005. Late Pleistocene eolian history of the Liwa region, Arabian Peninsula. Bull. Geol. Soc. Amer. 117, 1466-1480
- Suganuma, Y., Okada, M., Horie, K., Kaiden, H., Takehara, M., Senda, R., Kimura, J., Haneda, Y., Kawamura, K., Kazaoka, O., Head, M. J., 2015. Age of Matuyama-Brunhes boundary constrained by U-Pb zircon dating of a widespread tephra. Geology 43, 491-494.
- Timar-Gabor, A., Wintle, A. G., 2013. On natural and laboratory generated dose response curves for quartz of different grain sizes from Romanian loess. Quat. Geochron., 18, 34-40.
- Tripaldi, A., Forman, S. L., 2016. Eolian depositional phases during the past 50 ka and inferred climate variability for the Pampean Sand Sea, western Pampas, Argentina. Quat. Sci. Revs. 139, 77-93.
- Tsukamoto, S., Duller, G. A. T., Wintle, A. G., 2008. Characteristics of thermally transferred optically stimulated luminescence (TT-OSL) in quartz and its potential for dating sediments. Rad. Meas., 43(7), 1204-1218.
- Wang, X. L., Wintle, A. G., Lu, Y. C., 2006. Thermally transferred luminescence in fine-grained quartz from Chinese loess: Basic observations. Rad. Meas. 41(6), 649-658.
- Wang, X. L., Wintle, A. G., Lu, Y. C., 2007. Testing a single-aliquot protocol for recuperated OSL dating: Rad. Meas. 42(3), 380-391.
- Wiest, L. A., Forman, S. L., Mayhack, C., Lukens, W. E., Bassoo, R., Tew, V. T., Marin, L., Kocurek, G., 2020. A Large late Quaternary paleolake near Monahans, Texas, Inferred by large-scale biogenic structures. Geo. Soc. Amer Abstr. Prog. 52(2), https://doi.org/10.1130/abs/2019AM-337233.

- Wiest, L. A., Esker, D., Driese, S. G., 2016. The Waco Mammoth National Monument may represent a diminished watering-hole scenario based on preliminary evidence of post-mortem scavenging. Palaios 31, 592-606.
- Wiest, L. A., Esker, D., Driese, S. G., 2017. REPLY: The Waco Mammoth National Monument may represent a diminished watering-hole scenario based on preliminary evidence of postmortem scavenging. Palaios 32, 558-558.
- Wilkins, D.E., 1997. Hemiarid basin responses to abrupt climatic change: Paleolakes of the Trans-Pecos Closed Basin. Phys. Geogr. 18, 460-477
- Wilkins, D. E., Currey, D. R., 1997. Timing and extent of Late Quaternary Paleolakes in the Trans-Pecos closed basin, west Texas and south-central New Mexico. Quat. Res., 47, 306-315.
- Zander, A., Hilgers, A., 2013. Potential and limits of OSL, TT-OSL, IRSL and pIRIR₂₉₀ dating methods applied on a Middle Pleistocene sediment record of Lake El'gygytgyn, Russia:Climat. Past 9, 719-733.

Figure Captions

- Figure 1. (a) Study area on the Southern High Plains, USA showing occurrence of aeolian sand deposits. (b) Distribution of aeolian sand and dune fields on the Southern High Plains, showing the Monahans dune field. (c) Google Earth image of the Monahans dune field showing locations of Geoprobe cores.
- Figure 2. Four aeolian sedimentary facies A, B, C and D identified in Geoprobe cores from the Monahans dune field, TX.
- Figure 3. The stratigraphy of Geoprobe cores and one quarry exposure with the associated SAR-OSL and TT-OSL ages. Location of cores are shown on Figure 1.
- Figure 4. The percentage reduction of quartz grain TT-OSL compared to natural emissions (=1) by timed exposure from solar simulator Honle UVACUBE 400 at 1000 W/m².
- Figure 5. The comparison amongst TT-OSL solar resetting of quartz grains of sample BG4648 and previous evaluations of TT-OSL solar resetting of quartz grains.
- Figure 6. (a) The TT-OSL dose response curves, (b) the TT-OSL shine down curves, and (c) the radial plots of equivalent dose values for quartz extracts BG4595, BG4648, and BG4571.
- Figure 7. Comparison of luminescence ages on quartz grains by OSL-SAR and TT-OSL dating, showing 1σ errors.
- Figure 8. (a) Probability and kernel density distributions for forty-one luminescence ages >2 ka for the Monahans dune field and identified aeolian depositional periods (ADP) through finite method modelling with 2 σ errors. b) The four prominent ADPs (brown), two potential ADPs (light yellow) identified at one site, and with the occurrence of pluvial lakes (blue) in Pecos River and adjacent Rio Grande catchment, Lake King, (Wilkens and Currey, 1997) compared to the global marine oxygen isotope record for the past 600 ka. Numbers indicate the marine

oxygen isotope stages (Elderfield et al., 2013).





Facies A: A well-sorted often massive medium to fine aeolian sand to silty sand; distinct orange to yellowish-brown color. Aeolian reworked of older sediments time equivalent to Blackwater Draw Formation sediments. Sand sheet to interdune environments.



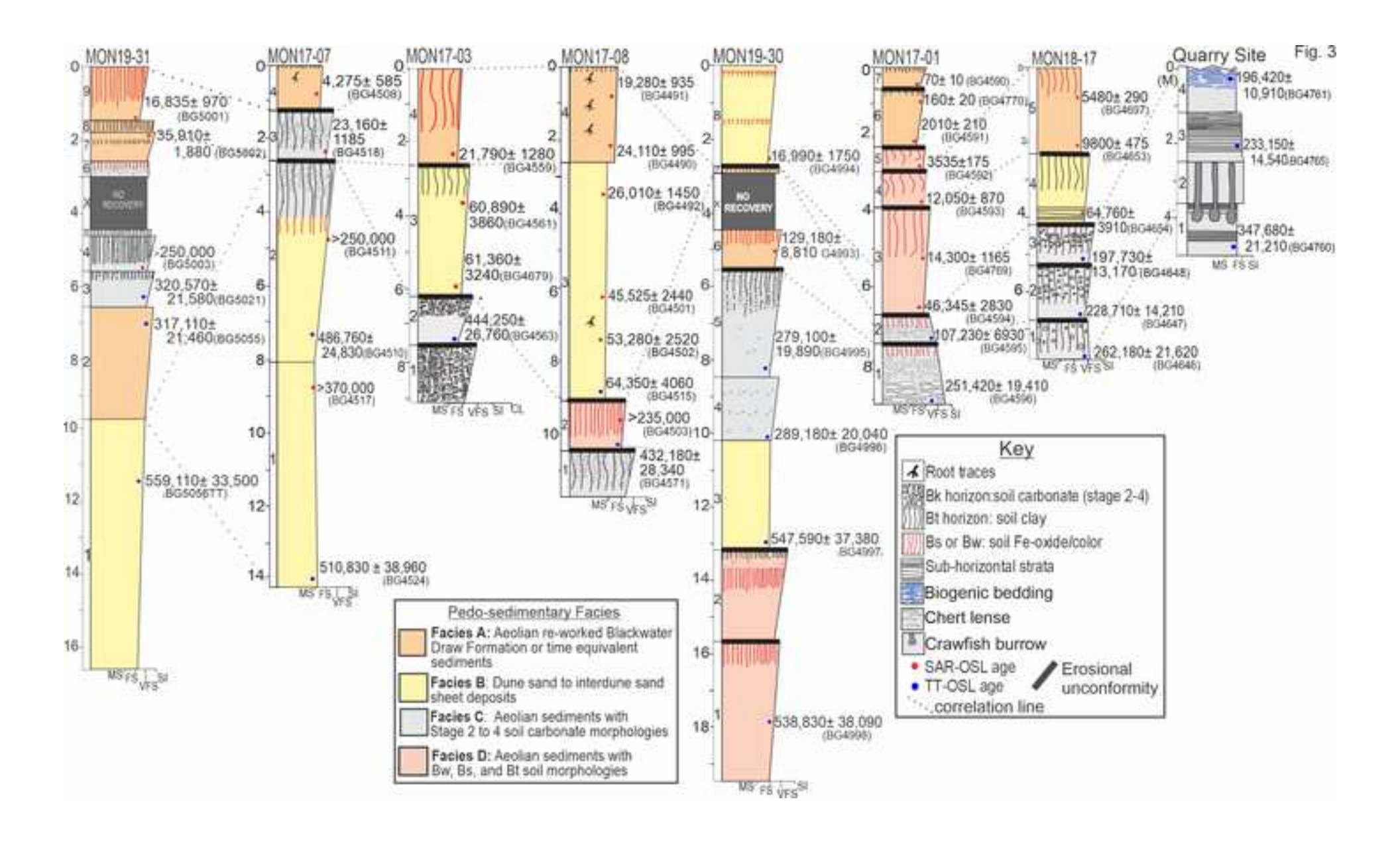
Facies B: A very well-sorted fine to medium aeolian sand <10% silt and clay, massive to mm to cm scale beds; distinctive light yellow to gray color. Primary aeolian sand, associated with dune movement and interdune environments.

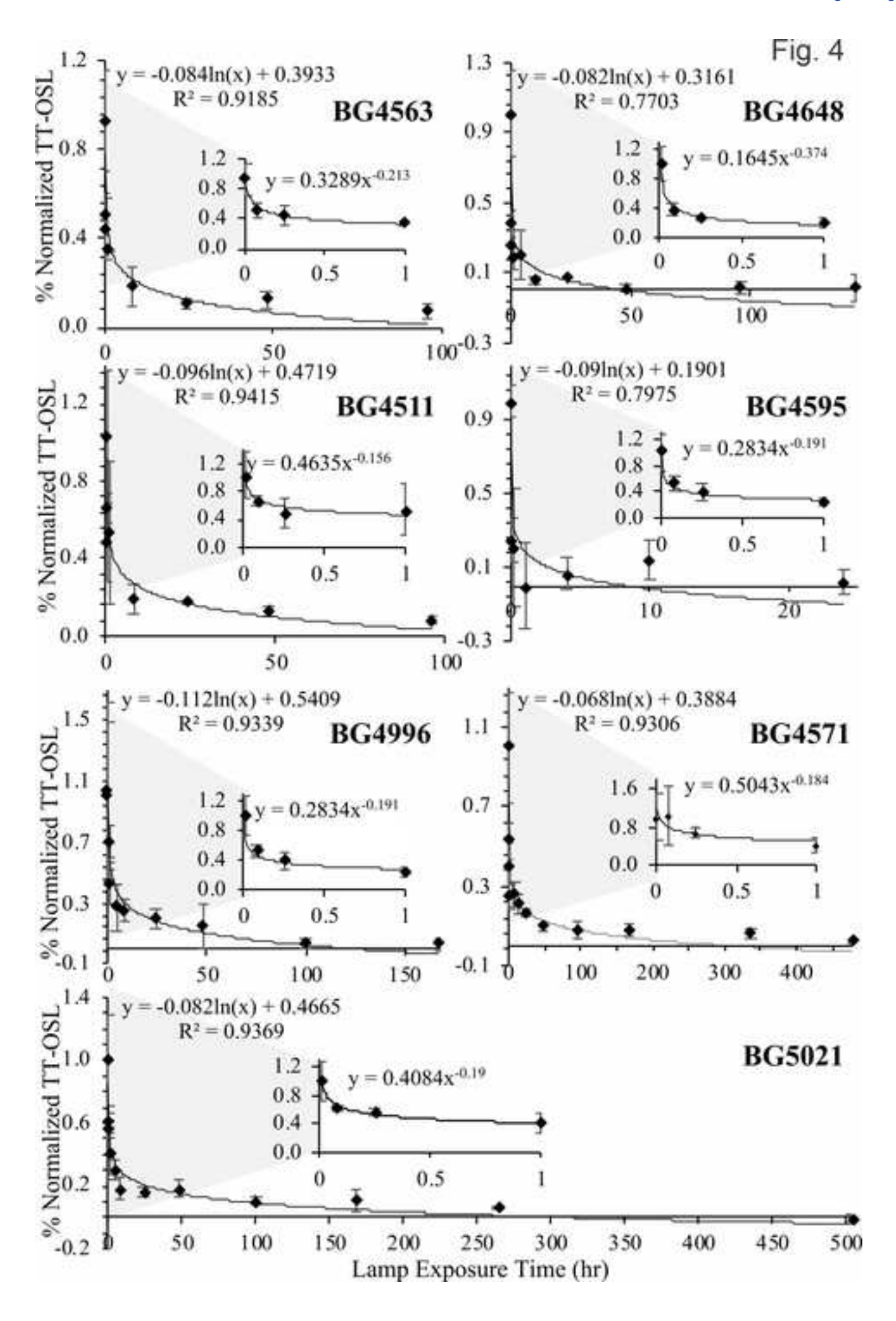


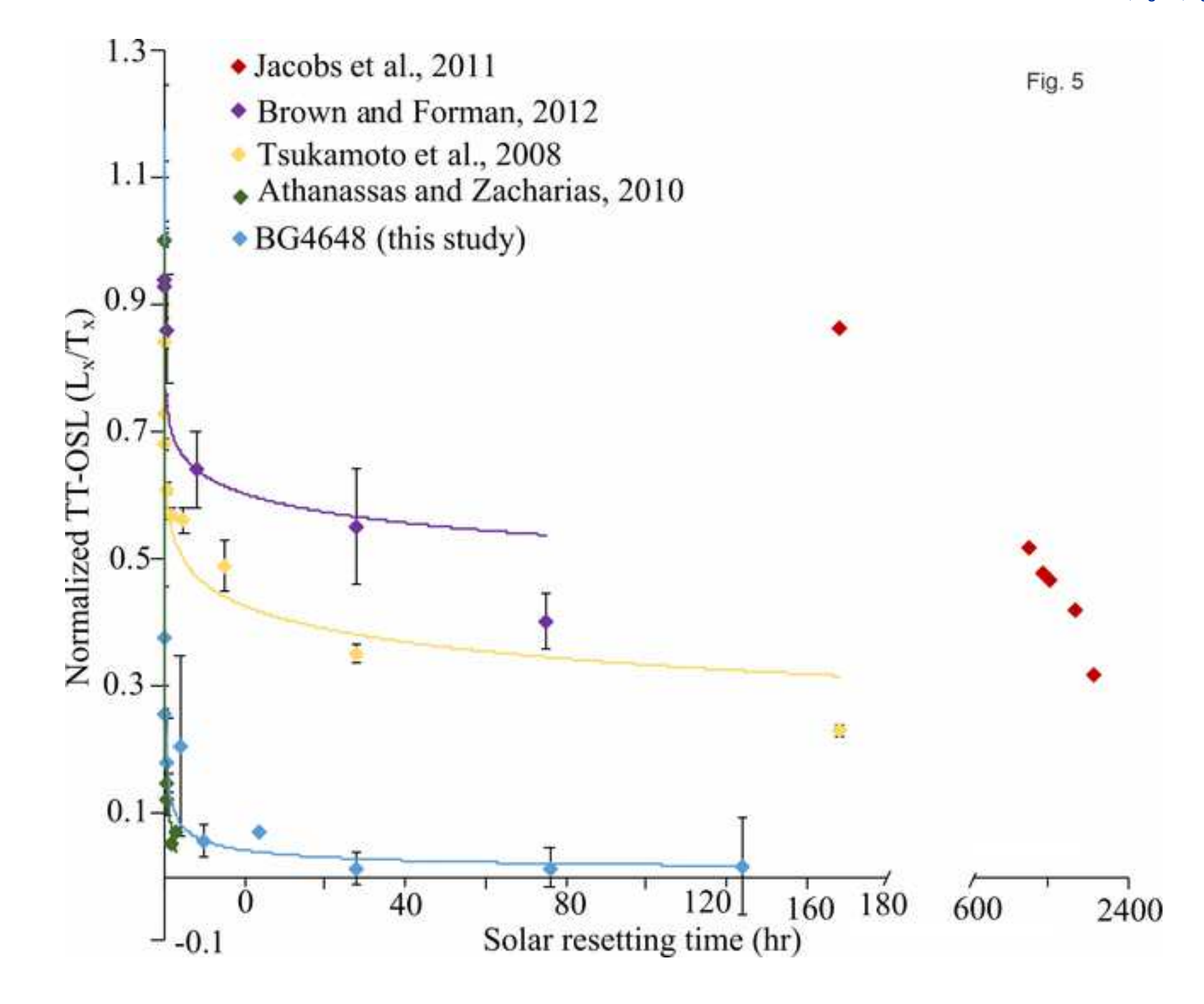
Facies C: A well-sorted fine to medium aeolian silty-sand to sandy mostly, massive with unit dominated by stage 2 to 4 carbonate morphology (Bk) with common nodules, induration with 15 to 55% carbonate content multiple welded, buried soils as a cumulic pedo-sedimentary complex.

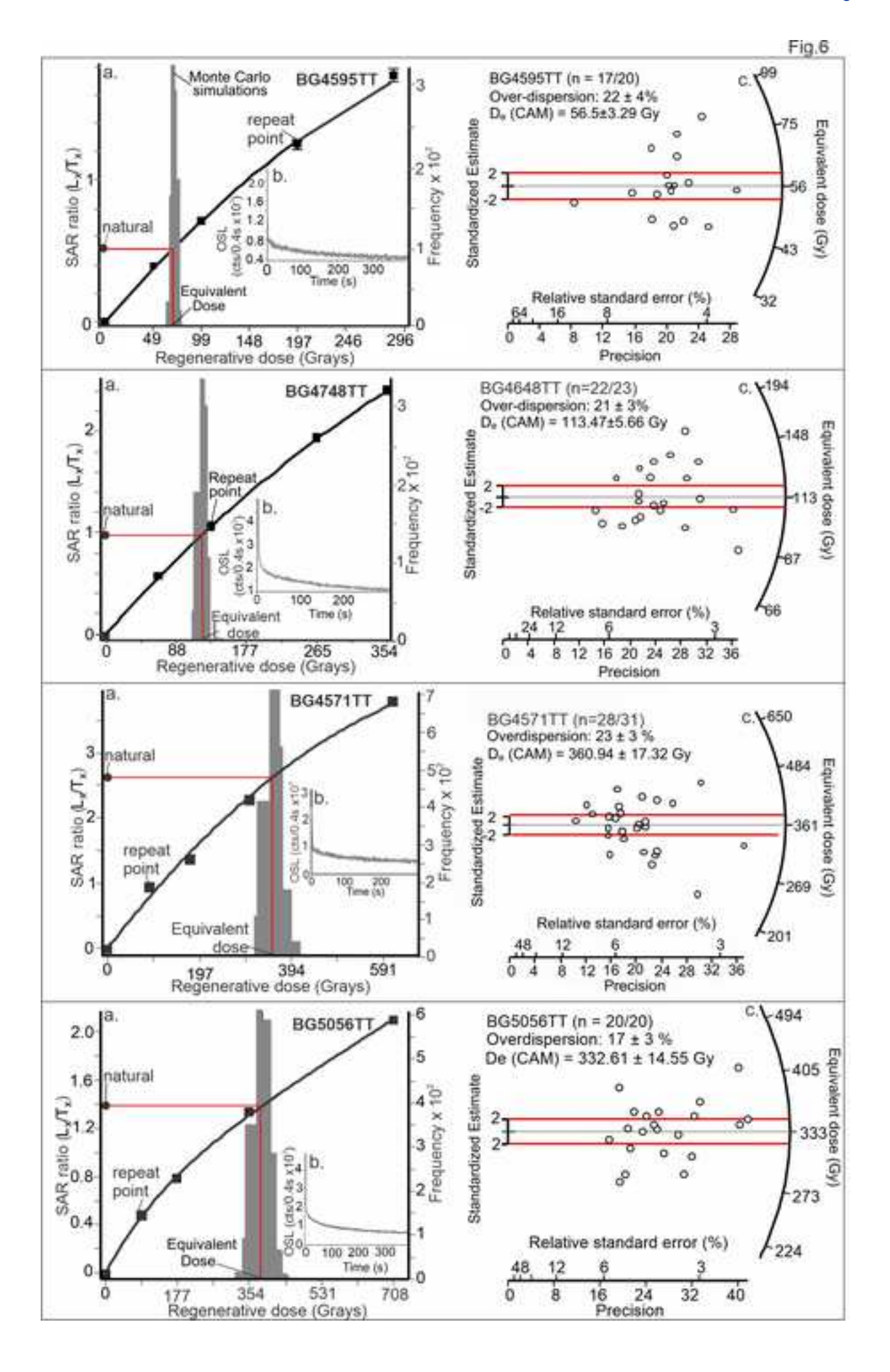


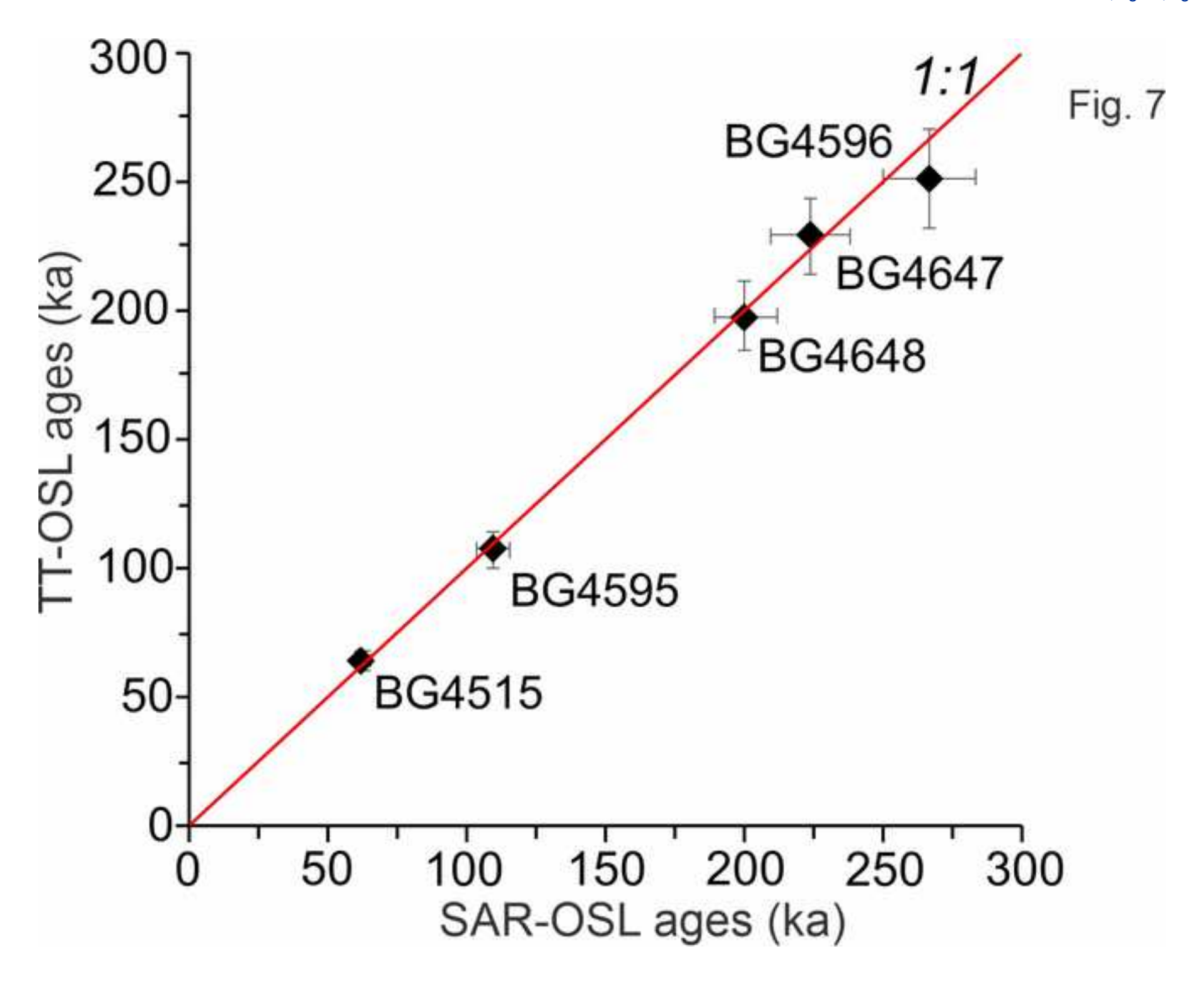
Facies D: A moderately well-sorted mostly massive aeolian silty sand to slightly silty sand with the unit dominated by variety of pedogenic features including Bw, Bs, and Bt horizons as a cumulic pedo-sedimentary complex.

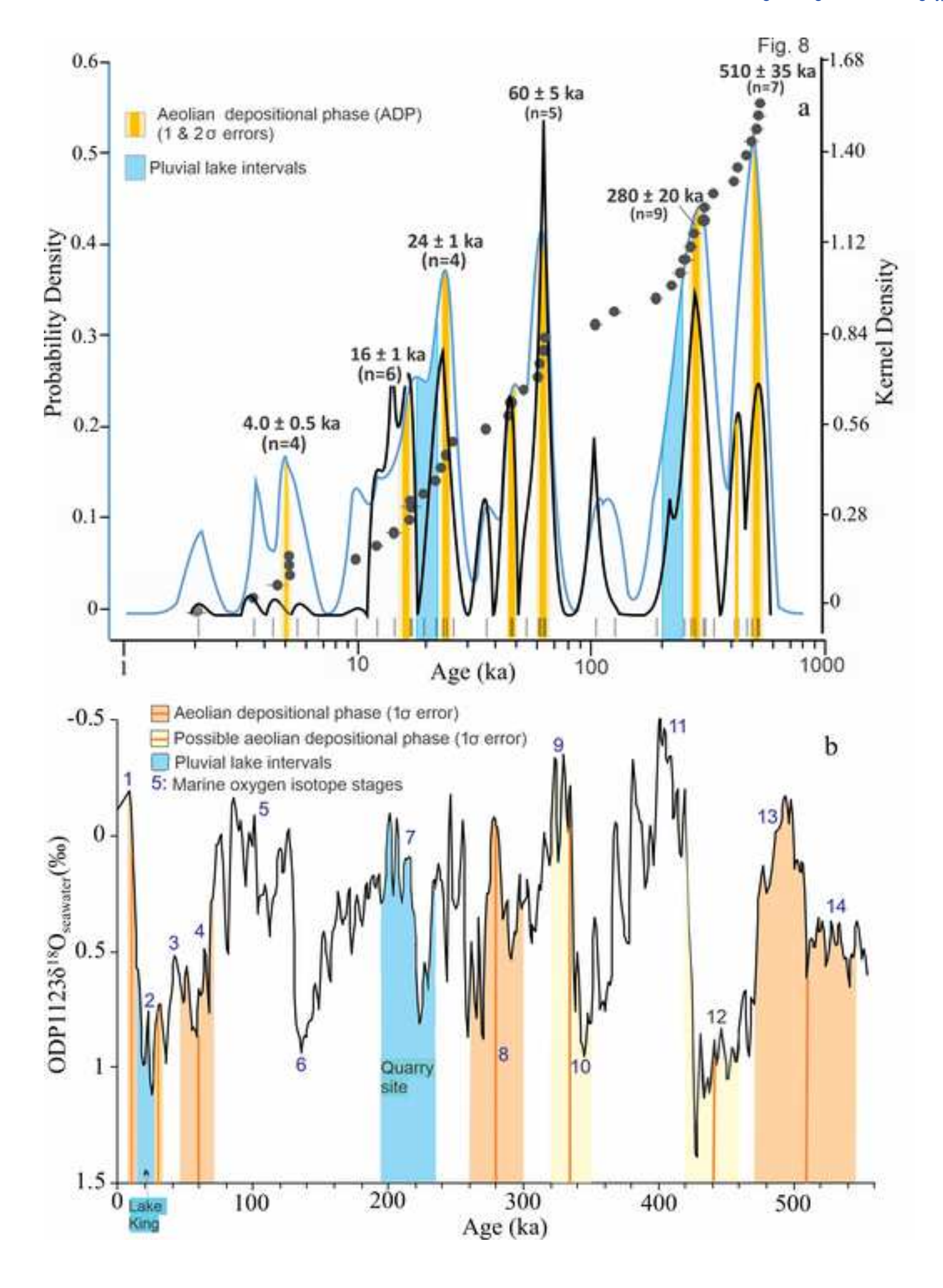












<u>*</u>

Table 1: Geoprobe cores location, top elevation and length adjacent to the Monahans dune field, TX

	Core/site location	Site surface	Core/site
	latitude (°N) and	elevation	length
Core/site	longitude (°W)	(m) ^a	(m)
Core MON17-01	31.67849, -102.83677	858.0	9.2
Core MON17-03	31.72651, -102.89083	867.2	9.1
Core MON17-07	31.67330, -102.92477	828.1	14.2
Core MON17-08	31.72012, -102.87481	869.8	11.7
Core MON18-17	31.64790, -102.91454	817.4	7.7
Core MON19-30	31.71722, -102.85280	876.6	19.3
Core MON19-31	31.69555, -102.83393	866.3	16.3
Quarry site	31.67147, -102.94838	823.6	4.9

^aElevation determined from GPS position from TNM data set at: https://apps.nationalmap.gov/elevation/##bottom

Table 2: Optically stimulated luminescence, single aliquot regeneration (OSL-SAR) and thermal transfer OSL (TT-OSL) ages on quartz grains from eolian sands, Monahans dune field, west Texas

			Grain	8	Over-	,	,			Cosmic		-
Core/drive/ depth	Lab		Size	Equivalent dose	dispersion				H_20	Dose rate	Dose rate	OSL
(cm)	numbera	Aliquotsb	, (μm)	(Gray) ^c	(%) ^d	U (ppm)e	Th (ppm)e	K (%)e	(%)	(mGray/yr)	(mGray/yr)	age (yr)f
MON17-1A 35	BG4590	49/55	250-150	0.05 ± 0.01	117 ± 12	0.42 ± 0.01	1.06 ± 0.01	0.18 ± 0.01	3 ± 1	0.249 ± 0.025	0.59 ± 0.02	70 ± 10
MON17-1A 50	BG4770	62/78	355-250	0.09 ± 0.01	48 ± 5	0.32 ± 0.01	0.88 ± 0.01	0.19 ± 0.01	5 ± 2	0.216 ± 0.022	0.52 ± 0.01	160 ± 20
MON17-1B 68	BG4591	41/42	250-150	1.00 ± 0.09	35 ± 4	0.34 ± 0.01	0.94 ± 0.01	0.18 ± 0.01	5 ± 2	0.191 ± 0.019	0.50 ± 0.02	2010 ± 210
MON17-1C 20	BG4592	32/34	250-150	2.35 ± 0.09	20 ± 3	0.48 ± 0.01	1.54 ± 0.01	0.30 ± 0.01	5 ± 2	0.176 ± 0.018	0.66 ± 0.02	3535 ± 175
MON17-1D 10	BG4593	33/35	250-150	7.00 ± 0.30	21 ± 3	0.47 ± 0.01	1.33 ± 0.01	0.23 ± 0.01	10 ± 2	0.149 ± 0.015	0.55 ± 0.02	$12,050 \pm 870$
MON17-1D 72	BG4769	54/60	355-250	7.17 ± 0.54	28 ± 3	0.38 ± 0.01	1.08 ± 0.01	0.26 ± 0.01	10 ± 2	0.147 ± 0.015	0.51 ± 0.02	$14,300 \pm 1165$
MON17-1F 15	BG4594	35/35	250-150	21.08 ± 1.04	20 ± 2	0.40 ± 0.01	1.09 ± 0.01	0.21 ± 0.01	10 ± 2	0.122 ± 0.012	0.45 ± 0.02	$46,345 \pm 2830$
MON17-1F 96	BG4595	30/35	250-150	58.65 ± 2.59	21 ± 3	0.49 ± 0.01	1.17 ± 0.01	0.28 ± 0.01	10 ± 2	0.112 ± 0.011	0.54 ± 0.02	$109,310 \pm 6090$
MON17-1F 96	BG4595TT	17/20	250-150	57.53 ± 3.35	22 ± 4	0.49 ± 0.01	1.17 ± 0.01	0.34 ± 0.01	10 ± 5	0.112 ± 0.011	0.54 ± 0.02	$107,230 \pm 6930$
MON17-IG 56	BG4596	31/35	250-150	110.79 ± 4.60	20 ± 3	0.38 ± 0.01	1.08 ± 0.01	0.21 ± 0.01	15 ± 5	0.103 ± 0.010	0.42 ± 0.02	$266,320 \pm 16,770$
MON17-IG 56	BG4596TT	16/17	250-150	104.87 ± 6.80	24 ± 4	0.38 ± 0.01	1.08 ± 0.01	0.21 ± 0.01	15 ± 5	0.103 ± 0.010	0.42 ± 0.02	$251,420 \pm 19,410$
MON17-3B 70	BG4559	34/34	250-150	13.92 ± 0.58	19 ± 2	0.49 ± 0.01	1.35 ± 0.01	0.26 ± 0.01	5 ± 2	0.192 ± 0.018	0.63 ± 0.02	$21,790 \pm 1280$
MON17-3D 60	BG4561	29/35	250-150	25.53 ± 1.21	23 ± 3	0.31 ± 0.01	0.92 ± 0.01	0.17 ± 0.01	10 ± 2	0.147 ± 0.015	0.42 ± 0.02	$60,890 \pm 3860$
MON17-3E 70	BG4679	37/40	250-150	33.76 ± 1.43	18 ± 2	0.51 ± 0.01	1.17 ± 0.01	0.25 ± 0.01	15 ± 5	0.130 ± 0.013	0.51 ± 0.02	$61,360 \pm 3240$
MON17-3F 93	BG4563	29/35	250-150	>230	NA	0.58 ± 0.01	4.45 ± 0.01	0.48 ± 0.01	15 ± 5	0.113 ± 0.011	0.89 ± 0.04	>250,000
MON17-3F 93	BG4563TT	18/20	250-150	397.50 ± 15.51	13 ± 3	0.58 ± 0.01	4.45 ± 0.01	0.48 ± 0.01	15 ± 5	0.113 ± 0.011	0.89 ± 0.04	$444,250 \pm 26,760$
MON17-7A 100	BG4508	72/75	250-150	4.93 ± 0.66	37 ± 3	0.81 ± 0.01	2.47 ± 0.01	0.64 ± 0.01	5 ± 2	0.214 ± 0.021	1.15 ± 0.03	4275 ± 585
MON17-7B 55	BG4518	35/35	250-150	22.78 ± 1.02	23 ± 3	0.79 ± 0.01	2.19 ± 0.01	0.56 ± 0.01	10 ± 2	0.184 ± 0.018	0.98 ± 0.03	$23,160 \pm 1185$
MON17-7D 83	BG4511	28/35	250-150	>268	NA	0.76 ± 0.01	3.38 ± 0.01	0.76 ± 0.01	10 ± 2	0.138 ± 0.014	1.07 ± 0.04	>250,000
MON17-7F 75	BG4510	5/5	250-150	>210	NA	0.53 ± 0.01	1.98 ± 0.01	0.47 ± 0.01	10 ± 2	0.109 ± 0.010	0.76 ± 0.02	>290,000
MON17-7F 75	BG4510TT	23/25	250-150	369.92 ± 16.71	17 ± 3	0.53 ± 0.01	1.98 ± 0.01	0.47 ± 0.01	10 ± 2	0.109 ± 0.010	0.76 ± 0.02	$486,760 \pm 24,830$
MON17-7G 70	BG4517	35/35	250-150	>210	NA	0.56 ± 0.01	1.99 ± 0.01	0.27 ± 0.01	10 ± 2	0.075 ± 0.007	0.56 ± 0.03	>370,000
MON17-7K 60	BG4524TT	20/20	250-150	289.19 ± 21.64	25 ± 5	0.58 ± 0.01	1.79 ± 0.01	0.38 ± 0.01	30 ± 5	0.066 ± 0.007	0.53 ± 0.02	$510,830 \pm 38,960$
MON17-8A 65	BG4491	34/35	250-150	11.97 ± 0.50	21 ± 3	0.52 ± 0.01	1.49 ± 0.01	0.22 ± 0.01	7 ± 2	0.208 ± 0.021	0.62 ± 0.02	$19,\!280 \pm 935$
MON17-8B 50	BG4490	33/35	250-150	14.42 ± 0.48	15 ± 2	0.52 ± 0.01	1.49 ± 0.01	0.27 ± 0.01	10 ± 2	0.175 ± 0.016	0.60 ± 0.02	$24,110 \pm 995$
MON17-8C 70	BG4492	33/35	250-150	12.86 ± 0.64	20 ± 3	0.38 ± 0.01	1.29 ± 0.01	0.19 ± 0.01	10 ± 2	0.166 ± 0.015	0.49 ± 0.01	$26,010 \pm 1450$
MON17-8E 70	BG4501	33/35	250-150	18.63 ± 0.81	22 ± 3	0.34 ± 0.01	0.90 ± 0.01	0.17 ± 0.01	10 ± 2	0.128 ± 0.013	0.41 ± 0.01	$45,525 \pm 2440$
MON17-8F 70	BG4502	33/35	250-150	22.61 ± 0.90	19 ± 2	0.35 ± 0.01	0.98 ± 0.01	0.20 ± 0.01	10 ± 2	0.115 ± 0.011	0.42 ± 0.01	$53,280 \pm 2520$
MON17-8G 70	BG4515	33/35	250-150	44.15 ± 1.55	17 ± 2	0.51 ± 0.01	1.46 ± 0.01	0.46 ± 0.01	10 ± 2	0.090 ± 0.009	0.70 ± 0.01	$62,080 \pm 2710$
MON17-8G 70	BG4515TT	27/35	250-150	44.84 ± 2.48	25 ± 4	0.51 ± 0.01	1.46 ± 0.01	0.46 ± 0.01	10 ± 2	0.090 ± 0.009	0.70 ± 0.01	$64,350 \pm 4060$
MON17-8H 40	BG4503	30/35	250-150	>162	NA	0.61 ± 0.01	2.20 ± 0.01	0.40 ± 0.01	15 ± 5	0.089 ± 0.009	0.64 ± 0.01	>235,000
MON17-8I 6	BG4571	21/23	250-150	>230	NA	0.65 ± 0.01	3.75 ± 0.01	0.52 ± 0.01	20 ± 5	0.087 ± 0.009	0.84 ± 0.04	>260,000
MON17-8I 6	BG4571TT	28/31	250-150	360.94 ± 17.32	23 ± 3	0.65 ± 0.01	3.75 ± 0.01	0.52 ± 0.01	20 ± 5	0.087 ± 0.009	0.84 ± 0.04	$432,180 \pm 28,340$
MON18-17A 60	BG4697	39/40	250-150	3.90 ± 0.11	19 ± 2	0.51 ± 0.01	1.41 ± 0.01	0.32 ± 0.01	7 ± 2	0.215 ± 0.022	0.71 ± 0.02	5480 ± 290
MON18-17B 55	BG4653	39/40	250-150	9.65 ± 0.40	23 ± 3	0.80 ± 0.01	2.02 ± 0.01	0.56 ± 0.01	10 ± 2	0.196 ± 0.020	0.98 ± 0.02	9800 ± 475
MON18-17D 07	BG4654	39/40	250-150	44.22 ± 1.88	23 ± 3	0.48 ± 0.01	1.16 ± 0.01	0.43 ± 0.01	15 ± 5	0.158 ± 0.016	0.68 ± 0.03	$64,760 \pm 3910$
MON18-17E 05	BG4648	35/40	250-150	114.17 ± 4.57	20 ± 3	0.42 ± 0.01		0.34 ± 0.01			0.57 ± 0.02	$199,960 \pm 11,250$
												•

			Grain		Over-					Cosmic		
Core/drive/ depth	Lab		Size	Equivalent dose	dispersion				H_20	Dose rate	Dose rate	OSL
(cm)	number ^a	Aliquots ^l	⁵ (μm)	(Gray) ^c	(%) ^d	U (ppm) ^e	Th (ppm) ^e	K (%)e	(%)	(mGray/yr)	(mGray/yr)	age (yr)f
MON18-17E 05	BG4648TT	22/23	250-150	113.47 ± 5.66	21 ± 3	0.42 ± 0.01	1.17 ± 0.01	0.34 ± 0.01	15 ± 5	0.137 ± 0.014	0.57 ± 0.02	$197,730 \pm 13,170$
MON18-17F 07	BG4647	37/40	250-150	151.32 ± 6.47	22 ± 3	0.62 ± 0.01	2.06 ± 0.01	0.37 ± 0.01	15 ± 5	0.123 ± 0.012	0.68 ± 0.02	$223,490 \pm 14,030$
MON18-17F 07	BG4647TT	19/19	250-150	154.86 ± 7.04	17 ± 3	0.62 ± 0.01	2.06 ± 0.01	0.37 ± 0.01	15 ± 5	0.123 ± 0.012	0.68 ± 0.02	$228,710 \pm 14,210$
MON18-17F 85	BG4646	20/44	250-150	>140	NA	0.98 ± 0.01	3.69 ± 0.01	0.62 ± 0.01	15 ± 5	0.112 ± 0.011	1.05 ± 0.03	>130,000
MON18-17F 85	BG4646TT	11/12	250-150	274.41 ± 17.59	20 ± 4	0.98 ± 0.01	3.69 ± 0.01	0.62 ± 0.01	15 ± 5	0.112 ± 0.011	1.05 ± 0.03	$262,180 \pm 21,620$
MON19-30B 70	BG4994	36/38	250-150	9.00 ± 0.87	33 ± 4	0.38 ± 0.01	1.11 ± 0.01	0.22 ± 0.01	5 ± 2	0.164 ± 0.013	0.53 ± 0.02	$16,990 \pm 1,750$
MON19-30D 40	BG4993	37/50	250-150	93.48 ± 4.45	18 ± 2	0.59 ± 0.01	1.71 ± 0.01	0.54 ± 0.01	15 ± 5	0.130 ± 0.016	0.72 ± 0.03	$129{,}180 \pm 8{,}810$
MON19-30F 75	BG4995	24/24	250-150	>85	NA	0.49 ± 0.01	1.49 ± 0.01	0.26 ± 0.01	15 ± 5	0.095 ± 0.010	0.50 ± 0.02	>190,000
MON19-30F 75	BG4995TT	24/24	250-150	138.51 ± 7.56	24 ± 4	0.49 ± 0.01	1.49 ± 0.01	0.26 ± 0.01	15 ± 5	0.095 ± 0.010	0.50 ± 0.02	$279{,}100 \pm 19{,}890$
MON19-30G 115	BG4996TT	27/27	250-150	212.60 ± 11.27	25 ± 4	0.60 ± 0.01	2.22 ± 0.01	0.52 ± 0.01	20 ± 5	0.081 ± 0.008	0.74 ± 0.03	$289,180 \pm 20,040$
MON19-30I 100	BG4997TT	29/30	250-150	329.94 ± 17.38	26 ± 4	0.54 ± 0.01	2.33 ± 0.01	0.42 ± 0.01	25 ± 5	0.065 ± 0.006	0.60 ± 0.03	$547,590 \pm 37,380$
MON19-30L 120	BG4998TT	19/20	250-150	341.73 ± 19.37	25 ± 4	0.70 ± 0.01	2.37 ± 0.01	0.52 ± 0.01	30 ± 5	0.045 ± 0.005	0.63 ± 0.03	$538,830 \pm 38,090$
MON19-31A 75	BG5001	38/40	250-150	14.77 ± 0.74	22 ± 3	0.67 ± 0.01	1.80 ± 0.01	0.47 ± 0.01	10 ± 2	0.207 ± 0.021	0.88 ± 0.03	$16,835 \pm 970$
MON19-31B 40	BG5002	39/40	250-150	35.22 ± 1.60	17 ± 2	1.07 ± 0.01	1.82 ± 0.01	0.51 ± 0.01	10 ± 2	0.197 ± 0.020	0.98 ± 0.03	$35,910 \pm 1880$
MON19-31D 81	BG5003	24/40	355-250	>150	NA	0.53 ± 0.01	1.86 ± 0.01	0.31 ± 0.01	15 ± 5	0.137 ± 0.014	0.65 ± 0.02	>250,000
MON19-31D 128	BG5021	18/20	250-150	>160	NA	0.89 ± 0.01	2.80 ± 0.01	0.93 ± 0.01	15 ± 5	0.131 ± 0.013	1.12 ± 0.05	>150,000
MON19-31D 128	BG5021TT	23/25	250-150	358.68 ± 17.58	22 ± 3	0.89 ± 0.01	2.80 ± 0.01	0.93 ± 0.01	15 ± 5	0.131 ± 0.013	1.12 ± 0.05	$320,570 \pm 21,580$
MON19-31E 75	BG5055TT	26/30	250-150	267.51 ± 12.84	21 ± 3	0.69 ± 0.01	2.43 ± 0.01	0.59 ± 0.01	20 ± 5	0.108 ± 0.011	0.84 ± 0.04	$317,110 \pm 21,460$
MON19-31H 70		20/20	250-150	332.61 ± 14.55	17 ± 3	0.89 ± 0.01		0.40 ± 0.01		0.081 ± 0.008		$559,110 \pm 33,500$
Optically stimulated luminescence (OSL) ages on quartz grains from paludal sediments, Quarry Site, near the Monahans dune field, west Texas												
MINE-1D/0.7	BG4761TT	20/25	250-150	185.03 ± 9.25	19 ± 4	2.20 ± 0.01	0.97 ± 0.01	0.22 ± 0.01	10 ± 2	0.223 ± 0.022	0.94 ± 0.03	$196,420 \pm 10,910$
MINE-1B/3.2	BG4765	13/15	250-150	>200	NA	5.10 ± 0.01	0.71 ± 0.01	0.19 ± 0.01	10 ± 2	0.161 ± 0.017	1.44 ± 0.03	>140,000
MINE-1B/3.2	BG4765TT	28/34	250-150	345.10 ± 19.35	28 ± 4	5.10 ± 0.01	0.71 ± 0.01	0.19 ± 0.01	10 ± 2	0.161 ± 0.017	1.44 ± 0.03	$233,\!150 \pm 14,\!540$
MINE-1E/4.7	BG4760	27/37	150-100	>200	NA	1.52 ± 0.01	2.32 ± 0.01	0.52 ± 0.01	15 ± 5	0.143 ± 0.014	1.03 ± 0.05	>190,000
MINE-1E/4.7	BG4760TT	25/25	150-100	346.92 ± 15.78	20 ± 3	1.52 ± 0.01	2.32 ± 0.01	0.52 ± 0.01	15 ± 5	0.143 ± 0.014	1.03 ± 0.05	$347,680 \pm 21,210$

^aLab numbers written with the suffix 'TT' were analyzed using Thermal Transfer Optically Stimulated Luminescence (TT-OSL); all other lab numbers are analyses by Optically Stimulated Luminescence, Single Aliquot Regeneration (OSL-SAR).

^bAliquots used in equivalent dose calculations versus original aliquots measured.

Equivalent dose calculated on a pure quartz fraction analyzed under blue-light excitation (470 ± 20 nm). The central age model was used to calculated equivalent dose when overdispersion values are <25% (at one sigma errors); the Minimum Age Model (four components) was used to determine equivalent dose when overdispersion values were > 25% (at one sigma errors) (Galbraith and Roberts, 2012; Peng and Forman, 2019).

 $[^]d$ Values reflects precision beyond instrumental errors; values of $\leq 25\%$ (at 1 sigma limit) indicate low dispersion in equivalent dose values and a unimodal distribution.

^eU, Th and K content analyzed by inductively-coupled plasma-mass spectrometry analyzed by ALS Laboratories, Reno, NV; U content includes Rb equivalent, which was determined. The cosmic dose rate was calculated from parameters in Prescott and Hutton (1994) and includes soft components (Peng and Forman, 2019).

fSystematic and random errors calculated in a quadrature at one standard deviation by the Luminescence Dating and Age Calculator (LDAC) at https://www.baylor.edu/geosciences/index.php?id=962356 (Peng and Forman, 2019). The datum year is AD 2010.

Conflict of Interest

Conflicts of Interest Statement

Manuscript title:	Late Quaternary stratigraphy, luminescence chronology and environmental change for the Monahans
dune field, Wink	kler County, West Texas, USA

The authors whose names are listed immediately below certify that they have NO affiliations with or involvement in any organization or entity with any financial interest (such as honoraria; educational grants; participation in speakers' bureaus; membership, employment, consultancies, stock ownership, or other equity interest; and expert testimony or patent-licensing arrangements), or non-financial interest (such as personal or professional relationships, affiliations, knowledge or beliefs) in the subject matter or materials discussed in this manuscript.

Author names:

Steven L. Forman, Victoria Tew-Todd, Connor Mayhack, Liliana Marin, Logan A. Wiest and Griffin Money

The authors whose names are listed immediately below report the following details of affiliation or involvement in an organization or entity with a financial or non-financial interest in the subject matter or materials discussed in this manuscript. Please specify the nature of the conflict on a separate sheet of paper if the space below is inadequate.

Author names:

No conflict of interests by any of the authors.

This statement is signed by all the authors to indicate agreement that the above information is true and correct (a photocopy of this form may be used if there are more than 10 authors):

Author's name (typed)	Author's signature	Date
Steven L. Forman	Steren L Form	11/9/2021
Victoria Tew-Todd	V Ten Told	11/9/2021
Connor Mayhack	[Maylah	11/9/2021
Liliana Marin	L. MARIN	11/9/2021
Logan A. Wiest	L Wiest	11/8/2021
Griffin Money	_ G MONEY	11/8/2021



Date: November 9, 2021

Dear editors of Aeolian Research,

Enclosed is the manuscript entitled "Late Quaternary stratigraphy, luminescence chronology and environmental change for the Monahans dune Field, Winkler County, West Texas, USA" authored by Steven L. Forman, Victoria Tew-Todd, Connor Mayhack, Logan A. Wiest and Griffin Money for consideration by *Aeolian Research* for review and publication. The results of this research have not been previously published and this journal is the sole review platform for this paper. Thank you for your editorial stewardship.

Appendix 1: Stratigraphic logs for Monahans Geoprobe cores

Click here to access/download **Supplementary Material**Appendix 1.Strat.Logs.revision.docx

Appendix 2

Click here to access/download **Supplementary Material**Appendix.2. OSL Dating

Methods.References.Added.docx